Review

International Journal of Modern Physics B
Vol. 26, No. 26 (2012) 1230013 (55 pages)

DOI: 10.1142/S0217979212300137

World Scientific
www.worldscientific.com

NANOSCALE SUPERCONDUCTIVITY

S. P. KRUCHININ

Bogolyubov Institute for Theoretical Physics,
National Academy Science of Ukraine,
03680 Kiev, Ukraine
sergeikruchinin@yahoo.com

H. NAGAO

Division of Mathematical and Physical Science,
Graduate School of Natural Science and Technology,
Kanazawa University,
Kakuma, Kanazawa 920-1192, Japan

Received 12 July 2012
Accepted 17 July 2012
Published 5 September 2012

We deal with the problem of nanoscale superconductivity. Nanoscale superconductivity remains to be one of the most interesting research areas in condensed mater. Recent technology and experiments have fabricated high-quality superconducting MgB_2 nanoparticles. We consider the two-band superconductivity in ultrasmall grains, by extending the Richardson exact solution to two-band systems, and develop the theory of interactions between nano-scale ferromagnetic particles and superconductors. The properties of nano-sized two-gap superconductors and the Kondo effect in superconducting ultrasmall grains are investigated as well. The theory of the Josephson effect is presented, and his application to quantum computing are analyzed.

Keywords: Nanoscale superconductivity; MgB_2 nanogranulas; magnetic dots; Kondo effect; quantum computer.

Contents

1. Introduction

Recent advances in nanoscience have demonstrated that fundamentally new physical phenomena are found, when systems are reduced in size to dimensions which become comparable to the fundamental microscopic lengths of the investigated material. Superconductivity is a macroscopic quantum phenomena, and it is therefore especially interesting to see how this quantum state is influenced when the samples are reduced to nanometer sizes. Recent developments in nanotechnologies and measurement techniques nowadays allow the experimental investigation of the magnetic and thermodynamic superconducting properties of mesoscopic samples in this regime.

In this review, we develop some theoretical models to describe such nanoscale superconducting systems and explore possible new experimental phenomena which we can predict based upon these theoretical models. In bulk samples, the standard Bardeen–Cooper–Schrieffer (BCS) theory gives a good description of the phe-

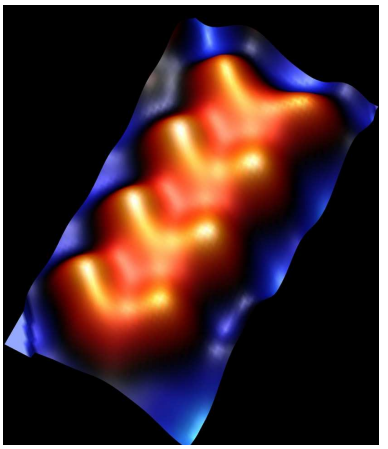

Fig. 1. The smallest superconductor in the world.

nomenon of superconductivity.[1] However, it was noticed by Anderson in 1959 that, as the size of a superconductor becomes smaller, and the quantum energy level spacing of the electrons in the sample approaches the superconducting gap, then the BCS theory will fail.[2] The exact solution to the reduced BCS Hamiltonian for finite-size systems was developed by Richardson in the context of nuclear physics a long time ago.[3] This shows that, while the grand canonical BCS wavefunction gives a very accurate solution of the BCS Hamiltonian in the limit where the number of electrons is very large $N \gg 1$, for small values of N, one has to use exact analytical methods to obtain reliable results.

The recent experimental advances in fabricating and measuring superconductivity in ultrasmall mesoscopic and nanoscale grains has renewed a theoretical interest in the Richardson solution.[4–7] Reference 10 shows the measurement for the smallest size of a superconductor in the world which is 5 A, Fig. 1.

Such systems are interesting for nanoelectronics and quantum computing.

In this review, we propose to develop theoretical models for nanoscale superconducting systems and to apply these models to a variety of systems of current experimental interest. The Richardson solution depends on the electron energy level spacings near to the Fermi level, and so these different geometric shapes will lead to different size dependences of the thermodynamic and electronic properties. Property small superconducting granules depends on the parity of the number of electrons N. By participating in Cooper pairing phenomenon has been called "the phenomenon of parity". Similar phenomena have long been known in nuclear physics. In 1992, the parity effect experimentally observed in a small granules of aluminum.

Experiments have recently demonstrated superconductivity in one-dimensional nanowires of lead[8] and carbon.[9] Our theoretical predictions will include the even–odd parity effects in tunneling spectra, which have already been observed on the

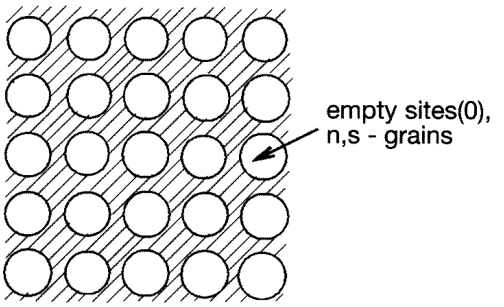

Fig. 2. Illustration of superconductor grains.

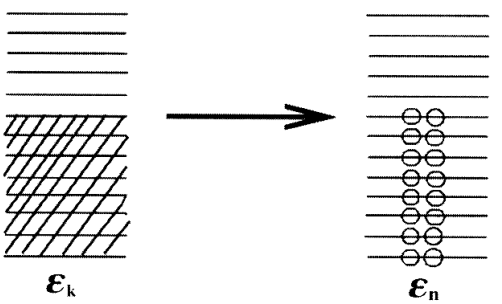

Fig. 3. Size effect in superconductor grains.

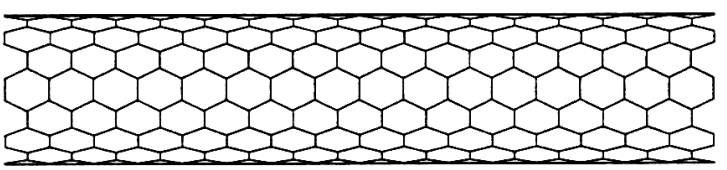

Fig. 4. Carbon nanotube revealing superconductivity.

nanometer scale in Al grains, (Fig. 2),[4] but which could also be observed in nanotube superconductors. In Figs. 2 and 3, we can see the ensemble of small metallic grains which can be in the normal or superconducting state. For such systems, the important parameters are the granular size (l), electron coherence length (ξ) and the penetration depth (λ).[10] In grains, there appears the quantum size effect (discretization of the electron energy spectrum). In Fig. 3, we show the size effect in grains. We note that the level spacing depends on many parameters such as the electron coherence length and the penetration depth.

Carbon nanotubes were first observed in 1991 by Iijima in Japan, Fig. 4.

Superconductivity was discovered in the simple binary compound MgB_2, in Ref. 18, with $T_c = 39$ K which is the highest temperature among the two-component systems. Magnesium diboride is reported to be an anisotropic superconductor with

conventional BCS electron–phonon coupling.[19] In the recent years, great efforts have been devoted to the fabrication of MgB_2 nanostructures that could play a crucial role in the field of applied superconductivity.[24] Recent technology and experiments have fabricated high-quality superconducting MgB_2 nanoparticles.

In this review, we investigate properties of nanosize two-gap superconductivity by using a two-sublevel model in the framework of the mean-field approximation. A model corresponding to a nanosize two-gap superconductivity is presented, and the partition function of the nanosize system is analytically derived by using the path integral approach. A definition of the critical level spacing of the two-gap superconductivity is also presented, and we discuss the condensation energy and the parity gap of two-gap superconductivity in relation to the size dependence of those properties with two bulk gaps and the effective pair scattering process between two sublevels. We present the theory of interactions between two nanoscale ferromagnetic particles embedded into a superconductor and spin orientation phase transitions in such a system. We also consider the ideas of quantum computing and quantum information in mesoscopic circuits. The theory of the Josephson effect is presented, and its applications in quantum computing are analyzed. The results of this chapter were obtained by the authors and published in works.[10,12–14]

2. Nanosize Superconductivity

Recent experiments[15,16] by Black *et al.* have also generated a high interest in the size dependence of the superconductivity. Properties of ultrasmall superconducting grains have been theoretically investigated by many groups.[17–23] In such ultrasmall grains, the old but fundamental theoretical question was noticed by Anderson.[2] The standard BCS theory gives a good description of the phenomenon of superconductivity in large samples. However, as the size of a superconductor becomes small, the BCS theory fails. In ultrasmall Al grains, the bulk gap has been discussed in relation to physical properties in ultrasmall grains such as the parity gap,[20] condensation energy,[23] electron correlation,[18] etc. with the size dependence of the level spacing[19] of samples.

Superconductivity was discovered in the simple binary compound MgB_2, in Ref. 18, with $T_c = 39$ K which is the highest temperature among the two-component systems. Magnesium diboride is reported to be an anisotropic superconductor with conventional BCS electron–phonon coupling.[19] The band structure of MgB_2 calculated in several works since the discovery superconductivity is similar to that of graphite and is formed by by the σ and π zones. The magnesium diboride has two superconducting gaps, 4 and 7.5 meV, due to the π and σ electron bands. The two-gap structure was established in a number of experiments,[19–25] and two-gap superconductivity has also discussed by many groups.[26–32]

In the recent years, great efforts have been devoted to the fabrication of MgB_2 nanostructures that could play a crucial role in the field of applied superconductivity.[24] The ideal candidate is one-dimensional (1D) nanostructures including nan-

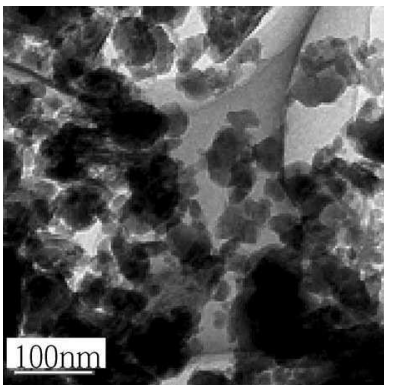

Fig. 5. TEM micrograph of 20–100 nm nanoparticles of MgB_2.

otubes, nanowires and nanoparticles. As for MgB_2, nanoparticles of approximately 40–100 nm in size are available (Fig. 5). For ultrasmall superconducting grains, the experiments[33,34] by Black *et al.* have also generated much interest in the size dependence of superconductivity. Properties of ultrasmall superconducting grains have been theoretically investigated by many groups.[35–39] Such ultrasmall grains were considered by Anderson.[40] The standard BCS theory gives a good description of the phenomenon of superconductivity in large samples. However, as the size of a superconductor becomes small, the BCS theory fails. For ultrasmall Al grains,[33,34] the bulk gap has been discussed in relation to physical properties of ultrasmall grains such as the parity gap,[38] condensation energy,[39] electron correlation,[36] etc., as well as the size-dependence of the level spacing[37] of samples. In this letter, we investigate the properties of two-gap superconductivity in a nano-sized system by using a two-sublevel model in the case of strong interaction.

We discuss the condensation energy and the parity gap of two-gap superconductivity in relation to the size-dependence of those properties in the case of two bulk gaps and the effective pair scattering. In this section, we investigate the properties of nanosize two-gap superconductivity by using a two-sublevel model in the framework of the mean-field approximation. A model corresponding to a nanosize two-gap superconductivity is presented, and the partition function of the nanosize system is analytically derived by using the path integral approach. A definition of the critical level spacing of the two-gap superconductivity is also presented, and we discuss the condensation energy and the parity gap of two-gap superconductivity in relation to the size dependence of those properties with two bulk gaps and the effective pair scattering process between two sublevels. In nanosize grains of a superconductor, the quantum level spacing approaches the superconducting gap. In the case of a two-gap superconductor, we can consider a model with two sublevels corresponding to two independent bands. In this section, we present a model for nanosize two-gap superconductivity and an expression for the partition function of the system.

In this section, we investigate the properties of nanosize two-gap superconductivity by using a two-sublevel model in the framework of the mean-field approximation. A model corresponding to a nanosize two-gap superconductivity is presented, and the partition function of the nanosize system is analytically derived by using the path integral approach. A definition of the critical level spacing of the two-gap superconductivity is also presented, and we discuss the condensation energy and the parity gap of two-gap superconductivity in relation to the size dependence of those properties with two bulk gaps and the effective pair scattering process between two sublevels. In nanosize grains of a superconductor, the quantum level spacing approaches the superconducting gap. In the case of a two-gap superconductor, we can consider a model with two sublevels corresponding to two independent bands. In this section, we present a model for nanosize two-gap superconductivity and an expression for the partition function of the system.

2.1. *Hamiltonian for nanosize grains*

We consider a pairing Hamiltonian with two sublevels corresponding to two bands 1 and 2 written as:

$$H = H_0 + H_{\text{int}}\,, \tag{1}$$

where

$$H_0 = \sum_{j,\sigma}[\varepsilon_{1j} - \mu]a^\dagger_{j\sigma}a_{j\sigma} + \sum_{k,\sigma}[\varepsilon_{2k} - \mu]b^\dagger_{k\sigma}b_{k\sigma}\,, \tag{2}$$

$$\begin{aligned} H_{\text{int}} = {} & -g_1 \sum_{j,j'\in I} a^\dagger_{j\uparrow}a^\dagger_{j\downarrow}a_{j'\downarrow}a_{j'\uparrow} - g_2 \sum_{k,k'\in J} b^\dagger_{k\uparrow}b^\dagger_{k\downarrow}b_{k'\downarrow}b_{k'\uparrow} \\ & + g_{12} \sum_{j\in I,k\in J} a^\dagger_{j\uparrow}a^\dagger_{j\downarrow}b_{k\downarrow}b_{k\uparrow} + g_{12} \sum_{j\in I,k\in J} b^\dagger_{k\uparrow}b^\dagger_{k\downarrow}a_{j\downarrow}a_{j\uparrow}\,. \end{aligned} \tag{3}$$

Here, $a^\dagger_{j\sigma}(a_{j\sigma})$ and $b^\dagger_{j\sigma}(b_{j,\sigma})$ are the creation (annihilation) operator in sublevels 1 and 2 with spin σ and the energies ε_{1j} and ε_{2j}, respectively, the operators for each sublevel satisfy the anticommutation relations and the operators between sublevels are independent, μ is the chemical potential, the second term in Eq. (1) is the interaction Hamiltonian, g_1 and g_2 are the effective interaction constant for sublevels 1 and 2, and g_{12} is an effective interaction constant which corresponds to the pair scattering process between two bands. The sums of j and k in Eq. (3) are over the set I of N_{1I} states corresponding to the half-filled band 1 with fixed width $2\omega_{1D}$ and the set J of N_{2J} states for band 2, respectively.

In this study, we assume that the Debye energies for two sublevels are the same: $\omega_{1D} = \omega_{2D} = \omega_D$. Within this assumption, N_{1I} and N_{2J} are relatively estimated by the density of state (DOS) for two bands as $N_{1I}/N_{2J} = \rho_1/\rho_2$, where ρ_1 and ρ_2 are DOS for two bands. The interaction constants g_1 and g_2 can be written as $d_1\lambda_1$ and $d_2\lambda_2$, respectively. $d_1 = 2\omega_D/N_{1I}$ and $d_2 = 2\omega_D/N_{2J}$ means the mean energy

level spacing, and λ_1 and λ_2 are the dimensionless parameters for two sublevels. We take the intersublevel interaction constant $g_{12} = \sqrt{d_1 d_2}\lambda_{12}$. In summary, we obtain a relation of $\rho_1/\rho_2 = N_{1I}/N_{2J} = d_2/d_1$.

2.2. *Path integral approach*

It is convenient to introduce a path integral approach for the treatment of fluctuations of the order parameters. This approach gives an exact expression for the grand partition function of a superconductor.

$$Z(\mu, T) = \mathrm{Tr} \exp\left[-\frac{H - \mu N}{T}\right], \tag{4}$$

where T is the temperature and N is the number operator in the grain. The idea of the path integral approach is to replace the description of a system under study in terms of electronic operators by an equivalent description in terms of the superconducting order parameter.

By the path integral approach, we obtain an expression for the grand partition function for the Hamiltonian (1):

$$Z(\mu, T) = \int D\Delta_1 D\Delta_1^* D\Delta_2 D\Delta_2^* e^{-S[\Delta_1, \Delta_2]}. \tag{5}$$

Here, the action $S[\Delta_1, \Delta_2]$ is defined as:

$$\begin{aligned} S[\Delta_1, \Delta_2] = &- \sum_j \left[\mathrm{Tr} \ln G_{1j}^{-1} - \frac{\xi_{1j}}{T}\right] - \sum_k \left[\mathrm{Tr} \ln G_{2k}^{-1} - \frac{\xi_{2k}}{T}\right] \\ &+ \int_0^{1/T} d\tau \frac{1}{g_1 g_2 - g_{12}^2} [g_2 |\Delta_1(\tau)|^2 + g_1 |\Delta_2(\tau)|^2 \\ &+ g_{12}(\Delta_1(\tau)\Delta_2(\tau)^* + \Delta_1(\tau)^* \Delta_2(\tau))]. \end{aligned} \tag{6}$$

Δ_1 and Δ_2 are bulk gaps for sublevels 1 and 2, respectively, $\xi_{1j} = \varepsilon_{1j} - \mu$ and $\xi_{2k} = \varepsilon_{2k} - \mu$, and the inverse Green's functions

$$G_{1j}^{-1}(\tau, \tau') = \left[-\frac{d}{d\tau} - \xi_{1j}\sigma^z - \Delta_1(\tau)\sigma^+ - \Delta_1^*(\tau)\sigma^-\right] \delta(\tau - \tau'), \tag{7}$$

and

$$G_{2k}^{-1}(\tau, \tau') = \left[-\frac{d}{d\tau} - \xi_{2k}\sigma^z - \Delta_2(\tau)\sigma^+ - \Delta_2^*(\tau)\sigma^-\right] \delta(\tau - \tau'), \tag{8}$$

where $\sigma^{\pm} = \sigma^x \pm i\sigma^y$ and $\sigma^{x,y,z}$ are the Pauli matrices. G_1^{-1} and G_2^{-1} satisfy antiperiodic boundary conditions.

In the case of a stronger interaction, $\Delta_1 \gg d_1$ and $\Delta_2 \gg d_2$, we consider the mean-field approximation for the order parameters in the path integral approach.

Substituting the time-independent order parameters into the action (6), we have:

$$\Omega(\mu) = \sum_j (\xi_{1j} - \epsilon_{1j}) + \sum_k (\xi_{2k} - \epsilon_{2k}) + \frac{1}{g_1 g_2 - g_{12}^2}[g_2\Delta_1^2 + g_1\Delta_2^2 + g_{12}(\Delta_1^*\Delta_2 + \Delta_1\Delta_2^*)]\,, \tag{9}$$

where $\epsilon_{1j} = (\xi_{1j}^2 + \Delta_1^2)^{1/2}$, and $\epsilon_{2k} = (\xi_{2k}^2 + \Delta_2^2)^{1/2}$. In Eq. (9), the values of Δ_1 and Δ_2 must be chosen in such a way which minimizes Ω. From the minimization of Ω, we obtain a coupled gap equation at zero temperature for the two-gap system:

$$\begin{pmatrix} \Delta_1 \\ \Delta_2 \end{pmatrix} = \begin{pmatrix} g_1 \sum_j \dfrac{1}{2\epsilon_{1j}} & -g_{12} \sum_k \dfrac{1}{2\epsilon_{2k}} \\ -g_{12} \sum_j \dfrac{1}{2\epsilon_{1j}} & g_2 \sum_k \dfrac{1}{2\epsilon_{2k}} \end{pmatrix} \begin{pmatrix} \Delta_1 \\ \Delta_2 \end{pmatrix}. \tag{10}$$

Fom the coupled gap equation, Eq. (10), we formally obtain an expression for the bulk gap for two-gap superconductivity at zero temperature:

$$\tilde{\Delta}_1 = \omega \sinh^{-1}\left(\frac{1}{\eta_1}\right) \tag{11}$$

and

$$\tilde{\Delta}_2 = \omega \sinh^{-1}\left(\frac{1}{\eta_2}\right), \tag{12}$$

where

$$\frac{1}{\eta_1} = \frac{\lambda_2 + \alpha_\pm[\eta_1, \eta_2]\lambda_{12}}{\lambda_1\lambda_2 - \lambda_{12}^2}, \tag{13}$$

$$\frac{1}{\eta_2} = \frac{\lambda_1 + \alpha_\pm^{-1}[\eta_1, \eta_2]\lambda_{12}}{\lambda_1\lambda_2 - \lambda_{12}^2} \tag{14}$$

and

$$\alpha_\pm\left[\eta_1, \eta_2\right] = \pm \frac{\sinh\left(\dfrac{1}{\eta_1}\right)}{\sinh\left(\dfrac{1}{\eta_2}\right)}. \tag{15}$$

For the two-band superconductivity, we can consider two cases for the phase of the gaps: $\mathrm{sgn}(\tilde{\Delta}_1) = \mathrm{sgn}(\tilde{\Delta}_2)$, and $\mathrm{sgn}(\tilde{\Delta}_1) = -\mathrm{sgn}(\tilde{\Delta}_2)$. For the same phase, α_+ is used in Eqs. (13) and (14), and we use α_- for the opposite phase. Note that $\tilde{\Delta}_1 = -\tilde{\Delta}_2$ in the limit of strong intersublevel coupling λ_{12}, that is, the opposite phase. For $\lambda_{12} = 0$, we find the same results for two bulk gaps derived from the conventional BCS theory for two independent sublevels.

2.3. *Condensation energy*

In this section, we discuss properties such as condensation energy, critical level spacing and parity gap of nanosize two-gap superconductivity by using the partition function derived in the previous section.

In nanosize superconductivity, the condensation energy can be defined as $E^C_{N,b}(\lambda) = E^G_{N,b}(0) - E^G_{N,b}(\lambda) - n\lambda d$, where $E^G_{N,b}$ is the ground state energy of the N-electron system in the interaction band, b is the number of electrons on single occupied levels and λ and n are the dimensionless coupling parameter and the number of pair occupied level, respectively. In the case of a nanosize two-band system, the condensation energy can be written as:

$$E^C_{N_1,b_1;N_2,b_2}(\lambda_1,\lambda_2,\lambda_{12}) = E^G_{N_1,b_1;N_2,b_2}(0,0,0) - E^G_{N_1,b_1;N_2,b_2}(\lambda_1,\lambda_2,\lambda_{12}) - n_1\lambda_1 d_1 - n_2\lambda_2 d_2\,, \tag{16}$$

where $E^G_{N_1,b_1;N_2,b_2}(\lambda_1,\lambda_2,\lambda_{12})$ means the ground state energy of (N_1+N_2)-electron system. From Eqs. (4) and (9), the condensation energy of the two-sublevel system can be expressed by the condensation energy of independent single level systems:

$$E^C_{N_1,b_1;N_2,b_2}(\lambda_1,\lambda_2,\lambda_{12}) = E^C_{N_1,b_1}(\lambda_1) + E^C_{N_2,b_2}(\lambda_2) - \frac{\lambda_{12}^2}{\lambda_1\lambda_2-\lambda_{12}^2} \times \left(\frac{\Delta_1^2}{d_1\lambda_1} + \frac{\Delta_2^2}{d_2\lambda_2} + \frac{2\left(\Delta_1^*\Delta_2+\Delta_1\Delta_2^*\right)}{\sqrt{d_1 d_2}\lambda_{12}}\right), \tag{17}$$

where $E^C_{N_1,b_1}(\lambda_1)$ and $E^C_{N_2,b_2}(\lambda_2)$ correspond to the condensation energy for the single band case. In the same phases of Δ_1 and Δ_2, the condensation energy (17) decreases, that is, there appears the instability by the coupling constant λ_{12}. On the other hand, in the opposite phases, the condensation energy becomes larger, because $\Delta_1^*\Delta_2 + \Delta_1\Delta_2^* < 0$. We can expect that the condensation energy for two-gap superconductivity leads to a higher stability, than that of two independent systems, due to the intersublevel coupling λ_{12} and the opposite phases.

2.4. *Critical level spacing*

To discuss the critical level spacing for a two-gap system, we start from the coupled gap Eq. (10). For the case of the critical level spacing of the two-gap system, we have:

$$1 = \lambda_1\sum_j \frac{1}{2|\tilde{\xi}_{1j}|} + \lambda_2\sum_k \frac{1}{2|\tilde{\xi}_{2k}|} - (\lambda_1\lambda_2-\lambda_{12}^2)\sum_j \frac{1}{2|\tilde{\xi}_{1j}|}\sum_k \frac{1}{2|\tilde{\xi}_{2k}|}\,, \tag{18}$$

where $\tilde{\xi}_i = \xi_i/d_i$ for sublevel $i = 1, 2$. For the odd or even cases, Eq. (18) can be approximately solved by using the digamma function: For the odd case, the critical level spacing becomes:

$$d^\circ_{1c} = \omega_D e^\gamma \exp\left[-\frac{1}{\lambda}\right], \quad d^\circ_{2c} = \frac{d_2}{d_1}d^\circ_{1c}\,, \tag{19}$$

and, for the even case,

$$d_{1c}^{e} = 4\omega_D e^{\gamma} \exp\left[-\frac{1}{\lambda}\right], \quad d_{2c}^{e} = \frac{d_2}{d_1} d_{1c}^{e}\,. \tag{20}$$

Here, we use

$$\frac{1}{\lambda} = \frac{1}{2x}\left[\lambda_1 + \lambda_2 - ax + \sqrt{(\lambda_1 - \lambda_2 - ax)^2 + 4\lambda_{12}^2}\right] \tag{21}$$

with

$$x = \lambda_1\lambda_2 - \lambda_{12}^2\,, \tag{22}$$

$$a = \log\frac{d_1}{d_2}\,. \tag{23}$$

From these expressions, we find some relations:

$$d_{1c}^{e} = 4d_{1c}^{\circ}, \quad d_{2c}^{e} = 4d_{2c}^{\circ} \tag{24}$$

and

$$d_{1/2c}^{\circ} \approx \frac{e^{\gamma}}{2} \exp\left[\frac{1}{\eta_{1/2}} - \frac{1}{\lambda}\right] \tilde{\Delta}_{1/2}. \tag{25}$$

In the case of $|\lambda_1 - \lambda_2| \gg \lambda_{12}$, Eq. (25) can be approximately rewritten as:

$$d_{1/2c}^{\circ} \approx \frac{e^{\gamma}}{2} \exp\left[\frac{\lambda_2 - \lambda_1 + 2\alpha\lambda_{12}}{\lambda_1\lambda_2 - \lambda_{12}^2}\right] \tilde{\Delta}_{1/2}\,. \tag{26}$$

On the other hand, in the limit of $|\lambda_1 - \lambda_2| \ll \lambda_{12}$, we have:

$$d_{1/2c}^{\circ} \approx \frac{e^{\gamma}}{2} \exp\left[\frac{(1+\alpha)\,\lambda_{12}}{\lambda_1\lambda_2 - \lambda_{12}^2}\right] \tilde{\Delta}_{1/2}\,. \tag{27}$$

For the case of $\lambda_{12} = 0$, Eq. (25) can be rewritten as $d_{1/2c}^{\circ} \approx \exp[\gamma]/2 \exp[1/\lambda_1 - 1/\lambda_2]\tilde{\Delta}_{1/2}$. Therefore, when the coupling constants λ_1 and λ_2 take the same value, we have a relation similar to that for a single level system: $d_{1/2c}^{\circ} \approx 0.89\tilde{\Delta}_{1/2}$. These results suggest the critical level spacing strongly depend upon λ_{12} and the difference between the effective interaction constants for sublevels. The relation in Eq. (24) is the same relation in the conventional nanosize BCS theory.

2.5. *Parity gap*

In this subsection, we consider a parity gap in the case of two-gap superconductivity in ultrasmall grains. In the case of two sublevel spacings, the chemical potential lies halfway between the highest occupied and the lowest unoccupied levels of a smaller level spacing in the half-filled case, as shown in Fig. 6(a).

We assume that $d_1 < d_2$ and that the numbers of occupied levels corresponding to each sublevel are n_1 and n_2, respectively. Then, the total number of electron becomes $N = 2n_1 + 2n_2$. When we consider $N = 2n_1 + 2n_2 + 1$, the chemical

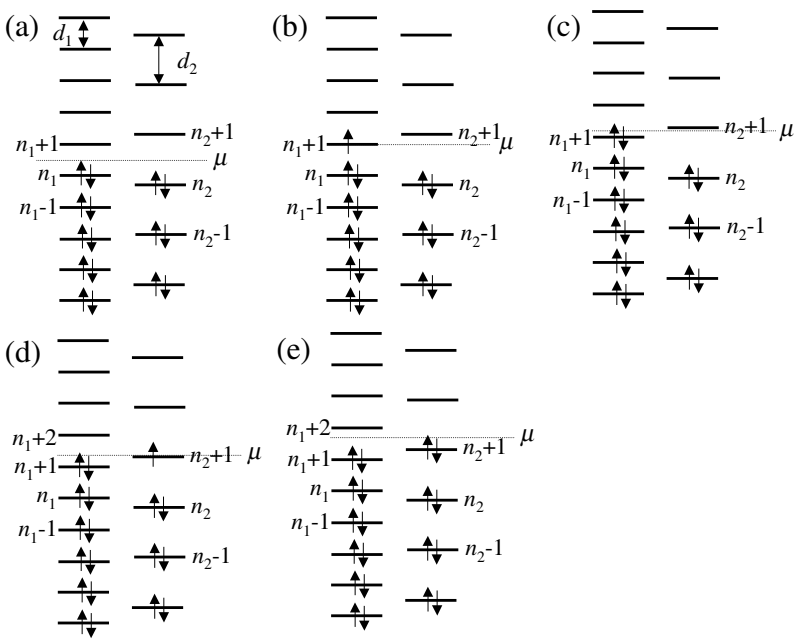

Fig. 6. Position of the chemical potential relative the electronic energy levels in a two-gap superconducting grain. Solid and dotted lines mean two sublevels. (a) Half-filled system with $2n_1 + 2n_2$ electrons. (b) $2n_1 + 1 + 2n_2$-electron system. (c) $2(n_1 + 1) + 2n_2$-electron system. (d) $2(n_1 + 1) + 2n_2 + 1$-electron system. (e) $2(n_1 + 1) + 2(n_2 + 1)$-electron system.

potential lies on the level ε_{1n_1+1}, as shown in Fig. 6(b). Figure 6(c) shows the position of the chemical potential in the case of $N = 2n_1 + 2n_2 + 2$. The parity gap of nanosize two-gap superconductivity is written as:

$$\Delta_p^1 = E^G_{2n_1+1+2n_2,1} - \frac{1}{2}(E^G_{2n_1+2n_2,0} + E^G_{2(n_1+1)+2n_2,0})\,. \tag{28}$$

From Eq. (9) and for the ground state energy $E^G_{N,b} = \Omega_{\mu_N} + \mu_N N$, we obtain:

$$\Delta_p^1 = \Delta_1 - \frac{d_1}{4}\left(\frac{\rho_1}{\rho_2} - 1\right)\,. \tag{29}$$

From Figs. 6(c), 6(d) and 6(e), we can define another parity gap:

$$\Delta_p^2 = E^G_{2(n_1+1)+2n_2+1,1} - \frac{1}{2}(E^G_{2(n_1+1)+2n_2,0} + E^G_{2(n_1+1)+2(n_2+1),0})\,. \tag{30}$$

From the latter definition of Eq. (30), we have:

$$\Delta_p^2 = \Delta_2 - \frac{d_2}{4}\left(\frac{3\rho_2}{\rho_1} - 1\right)\,. \tag{31}$$

The present results suggest two kinds of the dependence of the parity gap on the level spacing. The parity gap does not depend upon the effective interaction λ_{12}. The structure around the Fermi level plays an important role of the contribution to

the size dependence of the parity gap. We have investigated the properties of nanosize two-gap superconductivity by using a two-sublevel model in the framework of the mean-field approximation. From the discussion of the condensation energy in nanosize two-gap superconductivity, the phases of the gaps are very important to stabilize the superconductivity. In the same phases, the two-gap superconductivity is instable by the coupling constant λ_{12}. On the other hand, in the opposite phases, the superconductivity becomes stable. We can expect that, due to the condensation energy, the two-gap superconductivity becomes more stable than that for two independent systems due to the intersublevel coupling λ_{12} and the opposite phases.

We have also discussed the critical level spacing for two-gap superconductivity in ultrasmall grains. These results suggest that the critical level spacing strongly depends upon λ_{12} and the difference between the effective interaction constants for sublevels. Moreover, the relation between the critical level spacing and the bulk gaps is modified as compared with the result obtained for ultrasmall superconducting Al grains.

For the parity gap in two-gap superconductivity, the present results suggest two kinds of the dependence of the parity gap on the level spacing and that the structure around the Fermi level plays an important role by contributing to the size dependence on the parity gap. The parity gap does not depend upon the effective interaction λ_{12}.

In the case of a cluster system, we have to apply a more accurate approach beyond the mean-field approximation presented in this study by investigating the physical properties, and we also have to consider the contribution of the surface of samples to the level structure around the Fermi level. We will present these problems in the next section. On the basis of the presented results, we might expect the possibility of a new multi-gap superconductivity arising in the nanosize region with a higher critical transition temperature.

In summary, a model corresponding to a nanosize two-gap superconductivity has been presented, and an expression for the partition function of the nanosize system has been analytically derived by using the path integral approach. A definition of the critical level spacing of the two-gap superconductivity has been also presented, and we discuss the condensation energy and the parity gap of the two-gap superconductivity in relation to the size dependence of those properties with two bulk gaps, as well as the effective pair scattering process between two sublevels.

3. Exact Solution for the Superconductivity in Ultrasmall Grain

Many groups have theoretically investigated the physical properties such as critical level spacing, condensation energy, parity gap, etc. in ultrasmall grains with the conventional superconductivity.[17–23] The question concerning such nanosize superconducting grains has been discussed by Anderson.[2] The standard BCS theory becomes false, when the level spacing approaches the superconducting gap. To investigate the properties in such nanosize systems, it is necessary to take a

more accurate treatment. Braun and von Delft[21,22,24] have reintroduced the exact solution to the reduced BCS Hamiltonian developed by Richardson.[25–27] It is noteworthy that the Richardson's solution is applicable at distributions of single-electron energy levels. Gladilin *et al.*[23] have investigated the pairing characteristics such as the condensation energy, spectroscopic gap, parity gap, etc., by using the Richardson's exact solution for the reduced BCS Hamiltonian.

The recent discovery of superconductivity of MgB_2[28] with $T_c = 39$ K has also been much attracted a great interest aimed at the elucidation of its mechanism from both experimental and theoretical viewpoints. Since this discovery, the possibility of two-band superconductivity has also been discussed in relation to two gap functions experimentally and theoretically.

In this section, we investigate the two-band superconductivity in ultrasmall grains. The Richardson's exact solution is extended to two-band systems, and a new coupled equation is derived according to the procedure of Richardson's works. The parity gap and the condensation energy of an ultrasmall two-band superconducting grain are numerically given by solving the coupled equation. We discuss these properties of ultrasmall grains in relation to the correlation, interband interaction and size dependence.

3.1. *Exact solution for two-band superconductivity*

In this section, we derive an exact solution of the two-band superconductivity for a reduced BCS Hamiltonian.

3.2. *Hamiltonian*

We consider a Hamiltonian for two bands 1 and 2 written as:

$$H = H_1 + H_2 + H_{\rm int}\,, \tag{32}$$

where

$$H_1 = \sum_{j\sigma} \varepsilon_{1j} a^\dagger_{j\sigma} a_{j\sigma} - g_1 \sum_{jk} a^\dagger_{j\uparrow} a^\dagger_{j\downarrow} a_{k\downarrow} a_{k\uparrow}\,, \tag{33}$$

$$H_2 = \sum_{j\sigma} \varepsilon_{2j} b^\dagger_{j\sigma} b_{j\sigma} - g_2 \sum_{jk} b^\dagger_{j\uparrow} b^\dagger_{j\downarrow} b_{k\downarrow} b_{k\uparrow}\,, \tag{34}$$

$$H_{\rm int} = g_{12} \sum_{jk} a^\dagger_{j\uparrow} a^\dagger_{j\downarrow} b_{k\downarrow} b_{k\uparrow} + g_{12} \sum_{jk} b^\dagger_{j\uparrow} b^\dagger_{j\downarrow} a_{k\downarrow} a_{k\uparrow}\,. \tag{35}$$

The first and second terms of Eq. (32) correspond to the reduced BCS Hamiltonian for bands 1 and 2, respectively. The third term means a coupling between them and corresponds to the pair scattering process between these two bands (Fig. 7). $a^\dagger_{j\sigma}$ ($a_{j\sigma}$) and $b^\dagger_{j\sigma}$ ($b_{j\sigma}$) are the creation (annihilation) operator in bands 1 and 2 with spin σ and the single-particle levels ε_{1j} and ε_{2j}, respectively. The sums of j

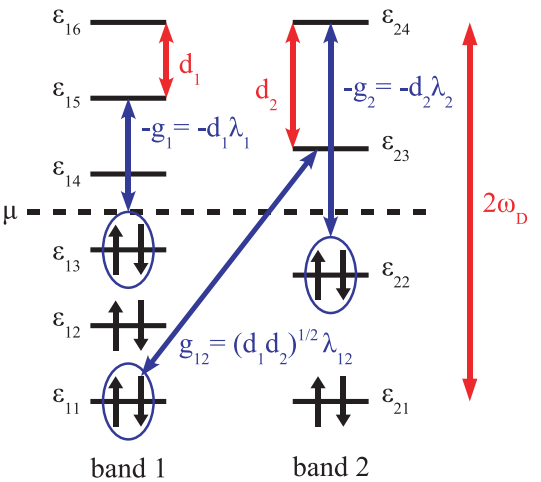

Fig. 7. Two-band system. The dotted line means the chemical potential; ε_{nj} is the single-particle energy for band n and level j; $-g_1$ and $-g_2$ are the intraband pair interaction coupling constants; g_{12} are the interband pair interaction coupling constant.

and k are taken over a set of N_1 states for band 1 with fixed width $2\hbar\omega_{1D}$ and a set of N_2 states for band 2 with fixed width $2\hbar\omega_{2D}$, respectively.

In this study, we assume that the Debye energies for two bands coincide with each other, i.e.,

$$\omega_{1D} = \omega_{2D} = \omega_D \,. \tag{36}$$

Within this assumption, N_1 and N_2 are relatively estimated by the DOS for two bands as:

$$\frac{N_1}{N_2} = \frac{\rho_1}{\rho_2} \,, \tag{37}$$

where ρ_1 and ρ_2 are DOS for two bands, respectively. The interaction constants g_1 and g_2 can be written as:

$$g_1 = d_1\lambda_1 \,, \quad g_2 = d_2\lambda_2 \,, \tag{38}$$

where d_1 and d_2 are the mean single-particle level spacing,

$$d_1 = \frac{2\hbar\omega_D}{N_1 - 1} \,, \quad d_2 = \frac{2\hbar\omega_D}{N_2 - 1} \,, \tag{39}$$

and λ_1 and λ_2 are the dimensionality interaction parameters for two bands. We define the interband interaction constant as:

$$g_{12} = \sqrt{d_1 d_2}\lambda_{12} \,. \tag{40}$$

In summary, we obtain the relation

$$\frac{\rho_1}{\rho_2} \approx \frac{N_1 - 1}{N_2 - 1} = \frac{d_2}{d_1} \,. \tag{41}$$

The system we are considering consists of two half-filled bands, each of which has equally spaced N_n single-particle levels and M_n ($= N_n/2$) doubly occupied pair levels ($n = 1, 2$). We take the single-particle level spacing as our energy unity. Thus, the single-particle spectrum is given by:

$$\varepsilon_{nj} = d_n j - \omega_D, \quad j = 1, 2, \ldots, N_n \quad (n = 1, 2)\,. \tag{42}$$

Richardson has obtained his solution within the single-band model for an arbitrary set of single-particle levels. For simplicity, we assume that there are no singly occupied single-particle levels. As can be seen from Eqs. (34)–(35), these levels are decoupled from the rest of the system. They are said to be blocked and contribute with their single-particle energies to the total energy. The above simplification implies that every single-particle level j is either empty (i.e., $|\text{vac}\rangle$), or occupied by a pair of electrons (i.e., $a^\dagger_{j\uparrow}a^\dagger_{j\downarrow}|\text{vac}\rangle$ and $b^\dagger_{j\uparrow}b^\dagger_{j\downarrow}|\text{vac}\rangle$). These are called as the unblocked level.

3.3. *Exact solution*

In order to extend Richardson's solution to a two-band system, we define two kinds of hard-core boson operators as:

$$c_j = a_{j\downarrow}a_{j\uparrow}, \quad c^\dagger_j = a^\dagger_{j\uparrow}a^\dagger_{j\downarrow}\,, \tag{43}$$

$$d_j = b_{j\downarrow}b_{j\uparrow}, \quad d^\dagger_j = b^\dagger_{j\uparrow}b^\dagger_{j\downarrow}\,, \tag{44}$$

which satisfy the commutation relations,

$$c^{\dagger 2}_j = 0, \quad [c_j, c^\dagger_k] = \delta_{jk}(1 - 2c^\dagger_j c_j), \quad [c^\dagger_j c_j, c^\dagger_k] = \delta_{jk}c^\dagger_j\,, \tag{45}$$

$$d^{\dagger 2}_j = 0, \quad [d_j, d^\dagger_k] = \delta_{jk}(1 - 2d^\dagger_j d_j), \quad [d^\dagger_j d_j, d^\dagger_k] = \delta_{jk}d^\dagger_j\,, \tag{46}$$

which reflects the Pauli principle for the fermions they constructed from.

Hamiltonian Eq. (32) for the unblocked levels can then be written as:

$$\begin{aligned} H_U = {} & 2\sum_j^{N_1}\varepsilon_{1j}c^\dagger_j c_j - g_1\sum_{jk}^{N_1}c^\dagger_j c_k + 2\sum_j^{N_2}\varepsilon_{2j}d^\dagger_j d_j - g_2\sum_{jk}^{N_2}d^\dagger_j d_k \\ & + g_{12}\sum_j^{N_1}\sum_k^{N_2}c^\dagger_j d_k + g_{12}\sum_j^{N_2}\sum_k^{N_1}d^\dagger_j c_k\,. \end{aligned} \tag{47}$$

We find the eigenstates $|M_1; M_2\rangle$ of this Hamiltonian with $M_1 + M_2$ pairs in the form

$$\begin{aligned} H_U|M_1; M_2\rangle_U &= E(M_1; M_2)|M_1; M_2\rangle_U \\ &= \left(\sum_{J=1}^{M_1}E_{1J} + \sum_{K=1}^{M_2}E_{2K}\right)|M_1; M_2\rangle_U\,, \end{aligned} \tag{48}$$

where $E(M_1; M_2)$ is the eigenvalue and

$$|M_1; M_2\rangle_U = \prod_{J=1}^{M_1} C_J^\dagger \prod_{K=1}^{M_2} D_K^\dagger |\text{vac}\rangle\,, \tag{49}$$

and

$$C_J^\dagger = \sum_j^{N_1} \frac{c_j^\dagger}{2\varepsilon_{1j} - E_{1J}}, \quad D_J^\dagger = \sum_j^{N_2} \frac{d_j^\dagger}{2\varepsilon_{2j} - E_{2J}}\,. \tag{50}$$

Now, we define $C_0^\dagger$ and $D_0^\dagger$ as:

$$C_0^\dagger = \sum_j^{N_1} c_j^\dagger, \quad D_0^\dagger = \sum_j^{N_2} d_j^\dagger\,. \tag{51}$$

Then we can rewrite Eq. (47) as:

$$\begin{aligned} H_U = {} & 2\sum_j^{N_1} \varepsilon_{1j} c_j^\dagger c_j - g_1 C_0^\dagger C_0 + 2\sum_j^{N_2} \varepsilon_{2j} d_j^\dagger d_j - g_2 D_0^\dagger D_0 \\ & + g_{12} C_0^\dagger D_0 + g_{12} D_0^\dagger C_0\,. \end{aligned} \tag{52}$$

The commutation relations for new operators are given as:

$$[c_j^\dagger c_j, C_J^\dagger] = \frac{c_j^\dagger}{2\varepsilon_{1j} - E_{1J}}, \quad [d_j^\dagger d_j, D_J^\dagger] = \frac{d_j^\dagger}{2\varepsilon_{2j} - E_{2J}}\,, \tag{53}$$

$$[C_0, C_J^\dagger] = \sum_j^{N_1} \frac{1 - c_j^\dagger c_j}{2\varepsilon_{1j} - E_{1J}}, \quad [D_0, D_J^\dagger] = \sum_j^{N_2} \frac{1 - d_j^\dagger d_j}{2\varepsilon_{2j} - E_{2J}}\,, \tag{54}$$

$$[H_U, C_J^\dagger] = E_{1J} C_J^\dagger + C_0^\dagger + g_1 C_0^\dagger \sum_j^{N_1} \frac{1 - c_j^\dagger c_j}{2\varepsilon_{1j} - E_{1J}} + g_{12} D_0^\dagger \sum_j^{N_1} \frac{1 - c_j^\dagger c_j}{2\varepsilon_{1j} - E_{1J}} \tag{55}$$

and

$$[H_U, D_J^\dagger] = E_{2J} D_J^\dagger + D_0^\dagger + g_1 D_0^\dagger \sum_j^{N_2} \frac{1 - d_j^\dagger d_j}{2\varepsilon_{2j} - E_{2J}} + g_{12} C_0^\dagger \sum_j^{N_2} \frac{1 - d_j^\dagger d_j}{2\varepsilon_{2j} - E_{2J}}\,. \tag{56}$$

Using the above-presented commutation relations, we find:

$$\begin{aligned} H_U |M_1; M_2\rangle_U = {} & \left(\sum_{J=1}^{M_1} E_{1J} + \sum_{K=1}^{M_2} E_{2K} \right) |M_1; M_2\rangle_U \\ & + C_0^\dagger \sum_{J=1}^{M_1} \left(1 - \sum_j^{N_1} \frac{g_1}{2\varepsilon_{1j} - E_{1J}} + \sum_{J' \neq J}^{M_1} \frac{2g_1}{E_{1J'} - E_{1J}} \right) |M_1(J); M_2\rangle_U \end{aligned}$$

$$+ D_0^\dagger \sum_{J=1}^{M_1} \left(\sum_j^{N_1} \frac{g_{12}}{2\varepsilon_{1j} - E_{1J}} - \sum_{J' \neq J}^{M_1} \frac{2g_{12}}{E_{1J'} - E_{1J}} \right) |M_1(J); M_2\rangle_U$$

$$+ C_0^\dagger \sum_{K=1}^{M_2} \left(\sum_j^{N_2} \frac{g_{12}}{2\varepsilon_{2j} - E_{2K}} - \sum_{K' \neq K}^{M_2} \frac{2g_{12}}{E_{2K'} - E_{2K}} \right) |M_1; M_2(K)\rangle_U$$

$$+ D_0^\dagger \sum_{K=1}^{M_2} \left(1 - \sum_j^{N_2} \frac{g_2}{2\varepsilon_{2j} - E_{2K}} + \sum_{K' \neq K}^{M_2} \frac{2g_2}{E_{2K'} - E_{2K}} \right)$$

$$\times |M_1; M_2(K)\rangle_U \,, \tag{57}$$

where

$$|M_1(L); M_2\rangle_U = \prod_{J=1}^{L-1} C_J^\dagger \prod_{J'=L+1}^{M_1} C_{J'}^\dagger \prod_{K=1}^{M_2} D_K^\dagger |\mathrm{vac}\rangle \,, \tag{58}$$

$$|M_1; M_2(L)\rangle_U = \prod_{J=1}^{M_1} C_J^\dagger \prod_{K=1}^{L-1} D_K^\dagger \prod_{K'=L+1}^{M_2} D_{K'}^\dagger |\mathrm{vac}\rangle \,. \tag{59}$$

Comparing Eq. (57) with Eq. (48), we obtain, for arbitrary J and K,

$$\begin{pmatrix} C_0^\dagger & D_0^\dagger \end{pmatrix} \begin{pmatrix} 1 + g_1 A_{1J} & -g_{12} A_{2K} \\ -g_{12} A_{1J} & 1 + g_2 A_{2K} \end{pmatrix} \begin{pmatrix} |M_1(J); M_2\rangle_U \\ |M_1; M_2(K)\rangle_U \end{pmatrix} = 0 \,, \tag{60}$$

where

$$A_{nL} = -\sum_j^{N_n} \frac{1}{2\varepsilon_{nj} - E_{nL}} + \sum_{L' \neq L}^{M_n} \frac{2}{E_{nL'} - E_{nL}} \,. \tag{61}$$

A nontrivial solution of Eq. (60) is derived from the determinantal equation

$$F_{JK} = (1 + g_1 A_{1J})(1 + g_2 A_{2K}) - g_{12}^2 A_{1J} A_{2K} = 0 \,. \tag{62}$$

This constitutes a set of $M_1 + M_2$ coupled equations for $M_1 + M_2$ parameters E_{1J} and E_{2K} ($J = 1, 2, \ldots, M_1; K = 1, 2, \ldots, M_2$), which may be thought of as self-consistently determined pair energies. Equation (62) is the exact eigenvalue equation for a two-band superconducting system and can be regarded as a generalization of the Richardson's original eigenvalue equation.

3.4. *Preprocessing for numerical calculations*

To remove the divergences from the second term of A_{nL} in Eq. (61), we make changes of the energy variables:

$$\begin{aligned} E_{n2\lambda} &= \xi_{n\lambda} + i\eta_{n\lambda} \,, \\ E_{n2\lambda-1} &= \xi_{n\lambda} - i\eta_{n\lambda} \,, \\ \lambda &= 1, 2, \ldots, M_n/2 \,, \end{aligned} \tag{63}$$

where we assume that the number of pairs is even. Since the complex pair energies appear in complex conjugate pairs, the total energy is kept in real.

A further transformation is necessary in order to remove the divergences from the first term of A_{nL}. We define new variables $x_{n\lambda}$ and $y_{n\lambda}$ as:

$$\xi_{n\lambda} = \varepsilon_{n2\lambda} + \varepsilon_{n2\lambda-1} + d_n x_{n\lambda} \quad (x_{n\lambda} \leq 0) \tag{64}$$

and

$$\eta_{n\lambda}^2 = -(\Delta\varepsilon_{n2\lambda}^2 - d_n^2 x_{n\lambda}^2) y_{n\lambda} \quad (y_{n\lambda} \geq 0)\,, \tag{65}$$

where

$$\Delta\varepsilon_{n2\lambda} = \varepsilon_{n2\lambda} - \varepsilon_{n2\lambda-1}\,. \tag{66}$$

Considering the sign of $y_{n\lambda}$, we can express $\eta_{n\lambda}$ as:

$$\begin{aligned} \eta_{n\lambda} &= |\eta_{n\lambda}| e^{-i\phi_{n\lambda}}, \\ \phi_{n\lambda} &= \begin{cases} 0 & \text{for} \quad \Delta\varepsilon_{n2\lambda}^2 - d_n^2 x_{n\lambda}^2 \leq 0\,, \\ \pi/2 & \text{for} \quad \Delta\varepsilon_{n2\lambda}^2 - d_n^2 x_{n\lambda}^2 > 0\,. \end{cases} \end{aligned} \tag{67}$$

Then we can rewrite F_{JK}, by using the new variables, and define the result as $F_{\alpha\beta}$. We extract the real and imaginary parts of $F_{\alpha\beta}$ as:

$$\begin{aligned} F_{\alpha\beta}^{+} = \frac{1}{2}(F_{\alpha\beta} + F_{\alpha\beta}^{*}) &= 1 + g_1 R_{1\alpha} + g_2 R_{2\beta} + (g_1 g_2 - g_{12}^2) R_{1\alpha} R_{2\beta} \\ &- (g_1 g_2 - g_{12}^2) I_{1\alpha} I_{2\beta} \cos(\phi_{1\alpha} + \phi_{2\beta}) \\ &- \{g_1 + (g_1 g_2 - g_{12}^2) R_{2\beta}\} I_{1\alpha} \sin\phi_{1\alpha} \\ &- \{g_2 + (g_1 g_2 - g_{12}^2) R_{1\alpha}\} I_{2\beta} \sin\phi_{2\beta}\,, \end{aligned} \tag{68}$$

$$\begin{aligned} F_{\alpha\beta}^{-} = \frac{1}{2i}(F_{\alpha\beta} - F_{\alpha\beta}^{*}) &= -(g_1 g_2 - g_{12}^2) I_{1\alpha} I_{2\beta} \sin(\phi_{1\alpha} + \phi_{2\beta}) \\ &+ \{g_1 + (g_1 g_2 - g_{12}^2) R_{2\beta}\} I_{1\alpha} \cos\phi_{1\alpha} \\ &+ \{g_2 + (g_1 g_2 - g_{12}^2) R_{1\alpha}\} I_{2\beta} \cos\phi_{2\beta}\,, \end{aligned} \tag{69}$$

where

$$\begin{aligned} R_{n\lambda} = &-\frac{2 d_n x_{n\lambda}(1 + y_{n\lambda})}{(1 - y_{n\lambda})^2 \Delta\varepsilon_{n2\lambda}^2 - (1 + y_{n\lambda})^2 d_n^2 x_{n\lambda}^2} \\ &+ 4 \sum_{\mu\neq\lambda}^{M_n} \frac{\xi_{n\mu\lambda}(\xi_{n\mu\lambda}^2 + \eta_{n\mu}^2 + \eta_{n\lambda}^2)}{(\xi_{n\mu\lambda}^2 + \eta_{n\mu}^2 + \eta_{n\lambda}^2)^2 - 4\eta_{n\mu}^2 \eta_{n\lambda}^2} \\ &- \sum_{j\neq 2\lambda-1,2\lambda}^{N_n} \frac{2\varepsilon_{n\lambda} - \xi_{n\lambda}}{(2\varepsilon_{n\lambda} - \xi_{n\lambda})^2 + \eta_{n\lambda}^2}\,, \end{aligned} \tag{70}$$

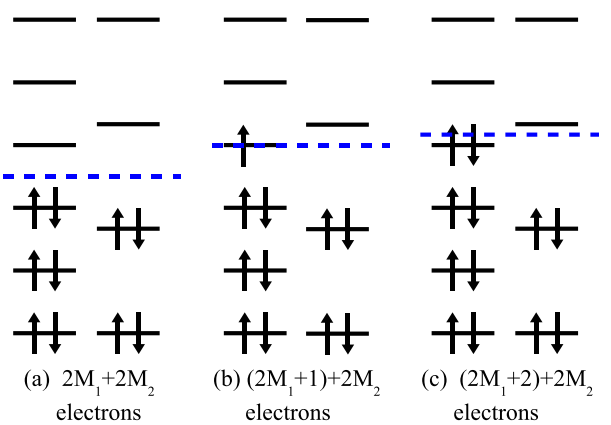

Fig. 8. Single-particle levels near the Fermi level in a the case of two-band superconductivity. The dotted lines mean the chemical potential. The left and right bands are band 1 and 2, respectively. d_1 and d_2 are the mean level spacings. (a) $2M_1 + 2M_2$ electron system, where M_n is a number of pair levels, (b) $(2M_1 + 1) + 2M_2$ electron system, (c) $(2M_1 + 2) + 2M_2$ electron system.

$$I_{n\lambda} = \Bigg\{ \frac{1 - y_{n\lambda}^2}{(1 - y_{n\lambda})^2 \Delta\varepsilon_{n2\lambda}^2 - (1 + y_{n\lambda})^2 d_n^2 x_{n\lambda}^2} - 4 y_{n\lambda} \sum_{\mu \neq \lambda}^{M_n} \frac{\xi_{n\mu\lambda}^2 - \eta_{n\mu}^2 + \eta_{n\lambda}^2}{\left(\xi_{n\mu\lambda}^2 + \eta_{n\mu}^2 + \eta_{n\lambda}^2\right)^2 - 4\eta_{n\mu}^2 \eta_{n\lambda}^2} + y_{n\lambda} \sum_{n \neq 2\lambda-1,2\lambda}^{N_n} \frac{1}{(2\varepsilon_{n\lambda} - \xi_{n\lambda})^2 + \eta_{n\lambda}^2} \Bigg\} \times \sqrt{\left| \frac{\Delta\varepsilon_{n2\lambda}^2 - d_n^2 x_{n\lambda}^2}{y_{n\lambda}} \right|} \tag{71}$$

and

$$\xi_{n\mu\lambda} = \xi_{n\mu} - \xi_{n\lambda} \,. \tag{72}$$

Therefore, for an arbitrary combination of α and β, we must solve the following equations:

$$\begin{aligned} &F_{\alpha\beta}^{+} = 0 \,, \\ &F_{\alpha\beta}^{-} = 0 \qquad (\alpha = 1, 2, \ldots, M_1/2; \quad \beta = 1, 2, \ldots, M_2/2) \,. \end{aligned} \tag{73}$$

3.5. *Results and discussion*

We now apply the exact solution for a two-band system to discuss the properties of the two-band superconductivity in ultrasmall grains. The single-particle level patterns of the $(2M_1 + m) + 2M_2$ electron system ($m = 0, 1$ and 2) under consideration are represented in Figs. 8(a), (b) and (c), respectively. The dotted lines mean the chemical potential, and d_1 and d_2 ($d_1 < d_2$) are the mean level spacings. As seen these figures, the additional electrons first occupy band 1 and then band 2.

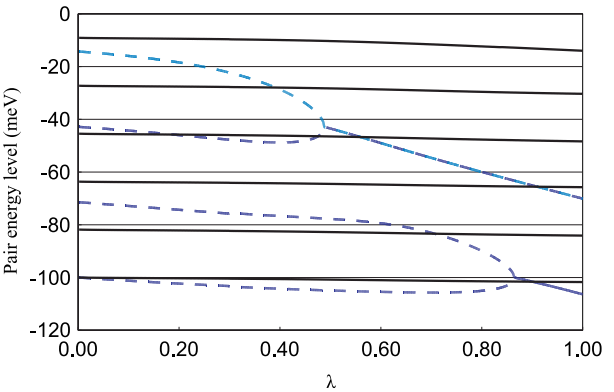

Fig. 9. Typical behavior of pair energy levels of two bands for the ground state. Parameters used in calculation are $N_1 = 12$, $N_2 = 8$, $M_1 = 6$, $M_2 = 4$, $\hbar\omega_D = 50$, $0 \leq \lambda_1 = \lambda_2 \leq 1.5$ and $0 \leq \lambda_{12} \leq 0.3$. Solid and broken lines correspond to the pair energy levels of band 1 and band 2, respectively.

Numerical calculations are carried out under the condition that $N_1 : N_2 = 3 : 2$, $\hbar\omega_D = 50$ and $\lambda_1 = \lambda_2 = \lambda$.

3.6. *Pair energy level*

By minimizing the sum of squares of Eqs.(68) and (69):

$$F = \sum_{\alpha=1}^{M_1/2} \sum_{\beta=1}^{M_2/2} (F_{\alpha\beta}^{+2} + F_{\alpha\beta}^{-2}) \tag{74}$$

for various interaction parameters, we obtain a behavior of pair energy levels E_{nJ} of two bands as shown in Fig. 9, in which the solid and broken lines correspond to the pair energy levels of band 1 and band 2, respectively. Parameters used in this calculation are $N_1 = 12$, $N_2 = 8$, $M_1 = 6$, $M_2 = 4$, $0 \leq \lambda \leq 1.0$ and $0 \leq \lambda_{12} \leq 0.2$.

As seen in the figures, band 2 condenses into degenerate levels, but the band 1 does not. In general, we can expect that the single-particle levels in a band, whose mean level spacing d is larger than that of the other band, degenerate faster. The behavior of the condensing band is qualitatively the same as that in the case of calculations for the single band.[22] The co-existence of the normal band and the condensed one may be reflected in the opposite phase of the gaps of these bands.[12]

3.7. *Condensation energy*

The condensation energy of band n for the $(2M_1 + m) + 2M_2$ electron system can be defined as:

$$E_n^C(2M_1 + m, 2M_2) = E_n(2M_1 + m, 2M_2) + \left(M_n + \frac{m}{2}\right) g_n - E_n^0(2M_1 + m, 2M_2)\,, \tag{75}$$

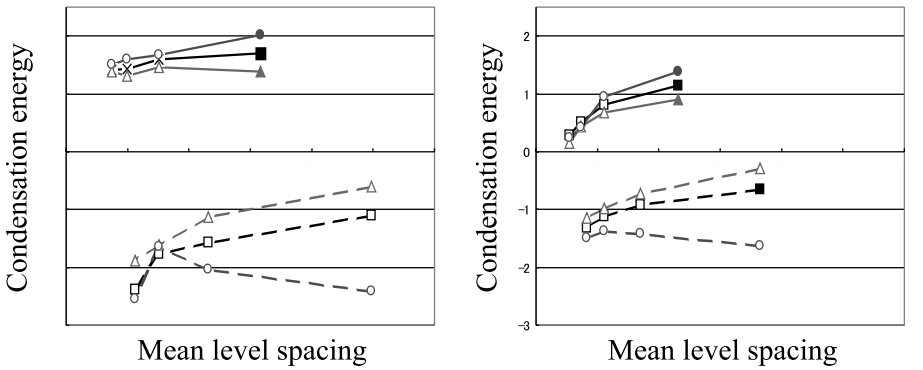

(a) (b)

Fig. 10. Condensation energy. Parameters used in calculation are $\hbar\omega_D = 50$, and $\lambda_1 = \lambda_2 = 0.5$. Values are normalized by the bulk gap, $\Delta_1 = \omega_D \sinh^{-1}(\lambda_2/(\lambda_1\lambda_2 - \lambda_{12}^2))$ or $\Delta_2 = \omega_D \sinh^{-1}(\lambda_1/(\lambda_1\lambda_2 - \lambda_{12}^2))$. The solid and broken lines correspond to the condensation energy for bands 1 and 2, respectively. Lines plotted by squares, by triangles, and by circles are for the $2M_1 + 2M_2$ electron system, for $(2M_1 + 1) + 2M_2$ electron system and for $(2M_1 + 2) + 2M_2$ electron system, respectively. (a) The condensation energy for the interband coupling parameter $\lambda_{12} = 0.01$. (b) The condensation energy for $\lambda_{12} = 0.1$.

where $E_n(2M_1 + m, 2M_2)$ and $E_n^0(2M_1 + m, 2M_2)$ are the ground state energies and the sum of the single-particle energies, respectively.

We calculate the condensation energies and show them in Figs. 10(a) and 10(b). The parameters used in this calculation are $\lambda = 0.5$ and $\lambda_{12} = 0.01$ for (a), $\lambda_{12} = 0.1$ for (b). Values are normalized by the bulk gap, $\Delta = \omega_D \sinh^{-1}(\lambda/(\lambda^2 - \lambda_{12}^2))$. The solid and broken lines correspond to the condensation energy for bands 1 and 2, respectively. Lines plotted by squares, by triangles and by circles are for the $2M_1 + 2M_2$ electron system, $(2M_1 + 1) + 2M_2$ electron system and $(2M_1 + 2) + 2M_2$ electron system, respectively.

As seen in the figures, we can understand that band 2 condenses, but band 1 does not because of the sign of values. This difference of signs may also be reflected in the opposite phases of the gaps of these bands. The behavior of the results for the condensed band (band 2) is qualitatively the same as in the case of the single-band calculations. The condensation energy of band 2 for the $(2M_1 + 2) + 2M_2$ electron system is, however, different from the others. We can also see that the condensation energy is affected by the interband interaction λ_{12}. This is mentioned in our previous work.[12]

3.8. *Parity gap*

The parity gap of band n is defined as:

$$\Delta_n^p = E_n(2M_1 + 1, 2M_2) - \frac{1}{2}\{E_n(2M_1, 2M_2) + E_n(2M_1 + 2, 2M_2)\}, \quad (76)$$

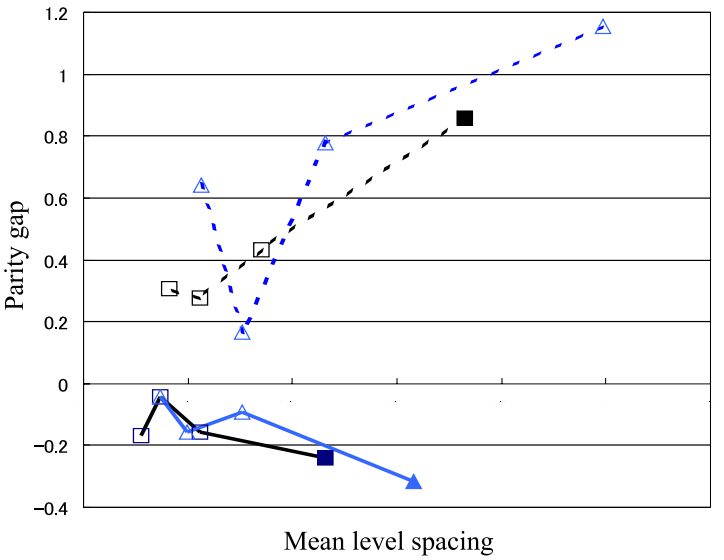

Fig. 11. Parity gap. Parameters used in calculation are $\hbar\omega_D = 50$, and $\lambda_1 = \lambda_2 = 0.5$. The solid and broken lines correspond to the parity gap for bands 1 and 2, respectively. Lines plotted by triangles and by squares are for the interband coupling parameter $\lambda_{12} = 0.01$ and for $\lambda_{12} = 0.1$, respectively. Values are normalized by the bulk gap.

which was introduced by Matveev and Larkin and characterizes the difference of even–odd ground state energies.[20]

We have also calculated the parity gaps shown in Fig. 11. The solid and broken lines correspond to the parity gap for bands 1 and 2, respectively. Lines plotted by triangles and by squares are for the interband coupling parameter $\lambda_{12} = 0.01$ and for $\lambda_{12} = 0.1$, respectively. Other parameters used in this calculation are the same as for the calculation of the condensation energy. Values are normalized by the bulk gap.

For the condensed band, we obtain qualitatively the same result as that in the case of the single-band calculations, i.e., there is a minimal point and a tendency toward 1 for $d \to 0$. The mean level spacing giving the minimal point is, however, much less than that for the case of calculations for the single band. The parity gap is almost independent of the interband interaction λ_{12}. This is also mentioned in our previous work.[12]

We have extended the Richardson's exact solution to the two-band system and have derived a new coupled equation. To investigate the properties of the two-band superconductivity, we have solved the equation numerically and have determined the behavior of pair energy levels, the condensation energy and the parity gap.

The band, whose mean level spacing is larger than that of the other band, degenerates and condenses faster. The behavior of the condensing band is qualitatively the same as that for the case of calculations for the single band. The co-existence

of the normal band and the condensed one may be reflected in the opposite phases of the gaps of these bands. This phase character appears in every of the results of numerical calculations. Therefore, the phase of a gap is important to stabilize the two-band superconductivity.

We have also calculated the condensation energy and the parity gap for two-band superconductivity. The results suggest that the interband interaction λ_{12} affects the condensation energy, but not the parity gap.

In summary, the expression of Richardson's exact solution for two-band superconductivity has been presented, by solving numerically a new coupled equation. Then, the behaviors of pair energy levels, the condensation energy and the parity gap have been determined. The results for the condensed band is almost qualitatively the same as those for the single band calculation and the co-existence of the normal band and the condensed one may be originated from the opposite phases of the gaps of these bands.

4. Kondo Effect Coupled to Superconductivity in Ultrasmall Grains

The Kondo effect has attracted a great interest, while considering the properties of semiconductor quantum dots. The Kondo effect can be understood as the magnetic exchange interaction between a localized impurity spin and free conduction electrons.[29] To minimize the exchange energy, the conduction electrons tend to screen the spin of the magnetic impurity and the ensemble forms a spin singlet. In a quantum dot, some exotic properties of the Kondo effect have been observed.[30,31] Recently, Sasaki *et al.* have found a significant Kondo effect in quantum dots with an even number of electrons.[32] The spacing of discrete levels in such quantum dots is comparable with the strength of the electron–electron Coulomb interaction. The Kondo effect in multilevel quantum dots has been investigated theoretically by several groups.[33–35] They have shown that the contribution from many levels enhances the Kondo effect in normal metals. There are some investigations on the Kondo effect in quantum dots revealing ferromagnetism,[36] noncollinear magnetism,[37] superconductivity[38] and so on.[39,40]

Properties of ultrasmall superconducting grains have been also theoretically investigated by many groups.[15–23,41] Black *et al.* have revealed the presence of a parity-dependent spectroscopic gap in the tunneling spectra of nanosize Al grains.[15,16] For such ultrasmall superconducting grains, the bulk gap has been discussed in relation to physical properties such as the parity gap,[20] condensation energy[21] and electron correlation[22] with the size dependence of the level spacing of samples.[23] In the previous works,[12] we have also discussed physical properties such as condensation energy, parity gap and electron correlation of two-gap superconductivity in relation to the size dependence and the effective pair scattering process. The possibility of new two-gap superconductivity has been also discussed by many groups.[42–51]

In a standard s-wave superconductor, the electrons form pairs with antialigned spins and are in a singlet state as well. When the superconductivity and the Kondo effect present simultaneously, the Kondo effect and the superconductivity are usually expected to be competing physical phenomena. The local magnetic moments from the impurities tend to align the spins of the electron pairs in the superconductor, which often results in a strongly reduced transition temperature. Buitelaar *et al.* have experimentally investigated the Kondo effect in a carbon nanotube quantum dot coupled to superconducting Au/Al leads.[38] They have found that the superconductivity of the leads does not destroy the Kondo correlations in the quantum dot at the Kondo temperature. A more subtle interplay has been proposed for exotic and not well-understood materials such as heavy-fermion superconductors, in which both effects might actually coexist.[52]

In this section, we investigate the Kondo effect and the superconductivity in ultrasmall grains by using a model which consists of the *sd* and reduced BCS Hamiltonians with the introduction of a pseudofermion. The mean-field approximation for the model is introduced and we calculate physical properties of the critical level spacing and the condensation energy. These physical properties are discussed in relation to the coexistence of both the superconductivity and the Kondo regime. Finally, we derive the exact equation for the Kondo regime in a nanosystem and discuss the condensation energy from the viewpoint of the correlation energy.

4.1. *Kondo regime coupled to superconductivity*

In nanosize superconducting grains, the quantum level spacing approaches the superconducting gap. It is necessary to treat the discretized energy levels of a small-sized system. For ultrasmall superconducting grains, we can consider the pairing-force Hamiltonian to describe the electronic structure of the system[27] and can determine the critical level spacing in the case where the superconducting gap function vanishes at a quantum level spacing.[23] In this section, we present a model for a system in the Kondo regime coupled to the superconductivity and discuss the physical properties such as critical level spacing and condensation energy by using the mean-field approximation in relation to the gap function, spin singlet order as the Kondo effect, coexistence and so on.

4.2. *Model*

We consider a model coupled to the superconductivity for quantum dots to investigate the Kondo effect in normal metals, which can be expressed by the effective low-energy Hamiltonian obtained by the Schrieffer–Wolff transformation:[53]

$$H = H_0 + H_1 + H_2\,, \tag{77}$$

where

$$H_0 = \sum_{k,\sigma} \varepsilon_k a^\dagger_{k\sigma} a_{k\sigma} + \sum_{\sigma} E_\sigma d^\dagger_\sigma d_\sigma\,, \tag{78}$$

$$H_1 = J\sum_{k,k'}[S_+ a^\dagger_{k'\downarrow}a_{k\uparrow} + S_- a^\dagger_{k'\uparrow}a_{k\downarrow} + S_z(a^\dagger_{k'\uparrow}a_{k\uparrow} - a^\dagger_{k'\downarrow}a_{k\downarrow})]\,, \tag{79}$$

$$H_2 = -g\sum_{k,k'} a^\dagger_{k\uparrow}a^\dagger_{k\downarrow}a_{k'\downarrow}a_{k'\uparrow}\,. \tag{80}$$

$a^\dagger_{k\sigma}$ ($a_{k\sigma}$) and $d^\dagger_\sigma$ (d_σ) are the creation (annihilation) operator corresponding to conduction electrons and the effective magnetic particle as an impurity, respectively. In this study, we assume the magnetic particle is a fermion with $S = 1/2$ for simplicity. E means an extraction energy given by $E_{\uparrow,\downarrow} = -E_0 \pm E_z$ included the Zeeman effect. The second term in Eq. (77) means the interaction between conduction electrons and the spin in a quantum dot. S is the spin operator as $S_+ = d^\dagger_\uparrow d_\downarrow$, $S_- = d^\dagger_\downarrow d_\uparrow$ and $S_z = (d^\dagger_\uparrow d_\uparrow - d^\dagger_\downarrow d_\downarrow)/2$. The third term corresponds to the interaction between conduction electrons included in the pairing force Hamiltonian.

Here, we introduce a pseudofermion for the magnetic particle operator[54] as:

$$\begin{aligned} d^\dagger_\uparrow &= f_\downarrow, \quad & d_\uparrow &= f^\dagger_\downarrow\,, \\ d^\dagger_\downarrow &= -f_\uparrow, \quad & d_\downarrow &= -f^\dagger_\uparrow\,. \end{aligned} \tag{81}$$

For this transformation, we have the condition:

$$f^\dagger_\uparrow f_\uparrow + f^\dagger_\downarrow f_\downarrow = 1\,, \tag{82}$$

and we have $|\sigma\rangle = f^\dagger_\sigma|0\rangle$. The spin operator S can be presented as $S_+ = f^\dagger_\uparrow f_\downarrow$, $S_- = f^\dagger_\downarrow f_\uparrow$ and $S_z = (f^\dagger_\uparrow f_\uparrow - f^\dagger_\downarrow f_\downarrow)/2$. The Hamiltonian can be rewritten as:

$$H_0 = \sum_{k,\sigma}\tilde{\varepsilon}_k c^\dagger_{k\sigma}c_{k\sigma} + \sum_\sigma E f^\dagger_\sigma f_\sigma\,, \tag{83}$$

$$H_1 = J\sum_{k,k',\sigma,\sigma'} f^\dagger_\sigma f_{\sigma'}c^\dagger_{k'\sigma'}c_{k\sigma}\,, \tag{84}$$

$$H_2 = -g\sum_{k,k'} c^\dagger_{k\uparrow}c^\dagger_{k\downarrow}c_{k'\downarrow}c_{k'\uparrow}\,, \tag{85}$$

where $c_{k\sigma} = \sum_i U_{ik}a_{i\sigma}$ with $\tilde{\varepsilon}_k = \sum_{i,j} U^\dagger_{ki}[\varepsilon_i\delta_{ij} - J/2]U_{jk}$. For the sake of simplicity, we only focus on $E_z = 0$ without an external magnetic field: $E = E_0$.

4.3. *Mean-field approximation*

In this section, we introduce the mean-field approximation for the present Hamiltonian (77). Eto *et al.* have presented the mean-field approximation for the Kondo effect in quantum dots.[55]

In the mean-field approximation, we can introduce the spin-singlet order parameter

$$\Xi = \frac{1}{\sqrt{2}}\sum_{k,\sigma}\langle f^\dagger_\sigma c_{k\sigma}\rangle\,. \tag{86}$$

This order parameter describes the spin couplings between the dot states and conduction electrons. The superconducting gap function can be expressed as:

$$\Delta = \sum_k \langle c_{k\downarrow} c_{k\uparrow} \rangle \,. \tag{87}$$

Using these order parameters in Eqs. (84) and (85), we obtain the mean-field Hamiltonian

$$H_{\rm MF} = \sum_{k,\sigma} \tilde{\varepsilon}_k c^\dagger_{k\sigma} c_{k\sigma} + \sum_\sigma \tilde{E} f^\dagger_\sigma f_\sigma + \sqrt{2} J \sum_{k,\sigma} [\Xi f_\sigma c^\dagger_{k\sigma} + \Xi^* c_{k\sigma} f^\dagger_\sigma]$$
$$- g \sum_k [\Delta^* c_{k\downarrow} c_{k\uparrow} + \Delta c^\dagger_{k\uparrow} c^\dagger_{k\downarrow}] \,. \tag{88}$$

Constraint (82) is taken into account by the second term with a Lagrange multiplier λ. In this study, we assume a constant DOS with the energy region of the Debye energy and the coupling constants can be expressed as $J = d\tilde{J}$ and $g = d\lambda$.

4.4. *Critical level spacing in the Kondo effect*

By minimizing the expectation value of $H_{\rm MF}$ in Eq. (88), the order parameters can be determined self-consistently. First, we show the Kondo effect without the pairing force part ($g = 0$) in the framework of the mean-field approximation. Next, the Kondo effect in the presence of the superconductivity is discussed in relation to the critical level spacing and the condensation energy. Finally, we derive the exact equation for the Kondo effect in ultrasmall grains coupled to normal metals and discuss properties such as the condensation energy in relation to Richardson's exact equation for the superconductivity.

For ultrasmall superconducting grains, the critical level spacing $d_c^{\rm BCS}$ can be expressed as $d_c^{\rm BCS} = 4\omega_D e^\gamma \exp(-1/\lambda)$ for even number of electrons, where ω_D means the Debye energy. This result suggests that the gap function of a nanosize system with the level spacing d vanishes, when the coupling parameter $\lambda_{\rm c}$ is less than the value $(\ln 4\omega_D/d + \gamma)^{-1}$. The bulk gap function $\Delta_{\rm c}$ with $\lambda_{\rm c}$ can be expressed as $\Delta_{\rm c} = \omega_D {\rm sh}^{-1}(1/\lambda_{\rm c})$.

Figure 12(a) shows the gap function of a nanosize system in the framework of the standard BCS theory. We can find the region where the gap function vanishes, when the coupling becomes less than $\lambda_{\rm c}$. This means the level spacing is larger than the gap function in this region.

Here, we drive the critical level spacing for only the Kondo regime ($\lambda = 0$). The equation determining the singlet order parameter can be expressed as:

$$\Xi = \sum_k \frac{\Xi(\xi_k - x)}{(\xi_k - x)^2 + \Xi^2} \,, \tag{89}$$

where $\xi_k = \tilde{\varepsilon}_k - \mu$, $x = [\tilde{\varepsilon}_k + \tilde{E} \pm \sqrt{(\tilde{\varepsilon}_k - \tilde{E})^2 + 4\Xi^2}]]/2$ and μ is the chemical potential. For the case of the critical level spacing, the solution shows that the

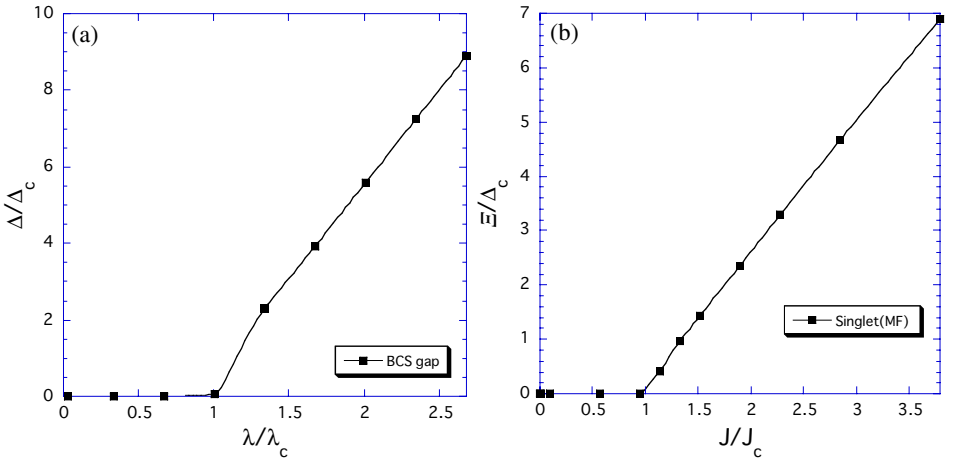

Fig. 12. Gap function and spin singlet order: (a) the gap function. The gap function vanishes in the region of λ values less than $\lambda_{\rm c}$. (b) Spin singlet order parameter. In the case of $\tilde{J} < \tilde{J}_{\rm c}$, the singlet order vanishes. The system consists of eight energy levels and eight electrons with the level spacing $d = 1.0$ and $\omega_D = 1.0$.

spin singlet order parameter vanishes. From Eq. (89), we can find the critical level spacing $d_{\rm c}^{\rm Kondo}$ for the Kondo regime.

$$d_{\rm c}^{\rm Kondo} = 4\omega_D e^{\gamma} \exp\left[-\frac{1}{2\sqrt{2}\tilde{J}}\right] . \tag{90}$$

When the coupling parameter $\tilde{J}$ is smaller than $\tilde{J}_{\rm c} = [2\sqrt{2}(\ln(4\omega_D/d) + \gamma)]^{-1}$, the spin singlet order parameter vanishes.

Figure 12(b) presents the spin singlet order parameter given by Eq. (86) in the case $g = 0$. In the region of $\tilde{J} < \tilde{J}_{\rm c}$, the order parameter vanishes. This result suggests the critical level spacing in the Kondo effect.

4.5. *Kondo effect coupled to the superconductivity*

Here, we consider a simple system which consists of eight energy levels and eight electrons and investigate the critical level spacing and the condensation energy of the coupled system between the superconductivity and the Kondo regime in the framework of the mean-field approximation of Eq. (88).

Figure 13(a) shows the spin singlet order parameter and the gap function for several cases. We can find the critical level spacings for the gap function and for the spin singlet order parameter. When $\lambda < \lambda_{\rm c}$ and $\tilde{J} > \tilde{J}_{\rm c}$, we can find only the spin singlet order parameters. In the region of $\lambda/\lambda_{\rm c}$ from 1.4 to 1.7 with $\tilde{J}/\tilde{J}_{\rm c} = 0.189$, we can find the coexistence of both the gap function and the spin singlet order parameter. For $\lambda/\lambda_{\rm c}$ larger than 1.7, only the gap function still exists and the spin singlet order parameter vanishes. At $\tilde{J}/\tilde{J}_{\rm c} = 0.284$, we can find the coexistence in the region $\lambda/\lambda_{\rm c} = 1.7 - 2.3$. These results suggest that strong local magnetic

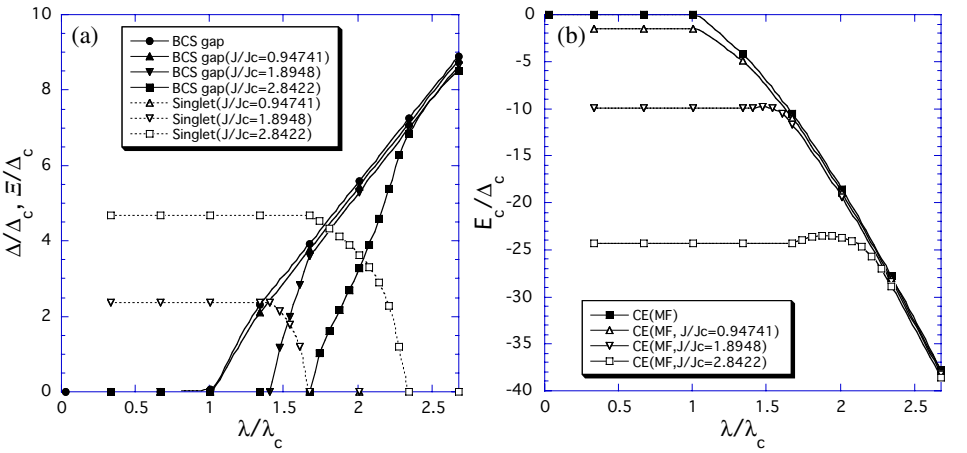

Fig. 13. Physical properties in a coupled system: (a) Gap function and spin singlet order parameter. (b) Condensation energy. $\tilde{J}/\tilde{J}_c = 0, 0.94741, 1.8948$ and 2.8422. Other parameters are the same.

moments from the impurities make the transition temperature for superconductivity to be reduced. However, the weak couplings λ of the superconductivity do not destroy the spin singlet order parameter at all. These results are in good agreement with the experimental results.[38] We can find that there is the coexistence region for both the superconductivity and the Kondo regime.

Figure 13(b) shows the condensation energy for several λ and $\tilde{J}$ values. We have found that the condensation energy of the coupled system between the superconductivity and the Kondo regime becomes lower than that for the pure superconductivity. In the coexistence region, the highest value of the condensation energy appears in all cases.

4.6. *Exact solution for the Kondo regime*

The standard BCS theory gives a good description of the phenomenon of superconductivity in large samples. However, when the size of a superconductor becomes small, the BCS theory fails. To investigate the physical properties such as the condensation energy, parity gap, etc., it is necessary to make a more accurate treatment. For the superconductivity in ultrasmall grains, the exact solution to the reduced BCS Hamiltonian presented by Richardson[27] has been applied to investigate the above-mentioned physical properties.[17]

By using the wavefunction describing all pair electron excitations, we can derive the exact solution for the pairing force (reduced) Hamiltonian

$$2 - \sum_{k=1}^{N} \frac{\lambda}{\tilde{\varepsilon}_k - E_i} + \sum_{l=1, l\neq i}^{n} \frac{2\lambda}{E_l - E_i} = 0\,, \tag{91}$$

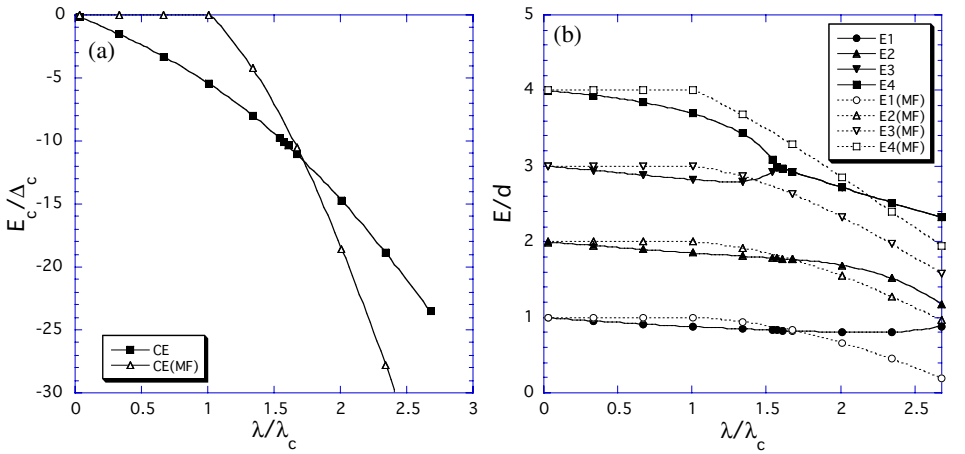

Fig. 14. Exact solution for the superconductivity: (a) Condensation energy of the exact solution and that obtained in the mean-field approximation (b) Pairing energy level with energy level obtained in the mean-field approximation. 8 energy levels, 8 electrons, $d = 1.0$, $\omega_D = 4.0$.

where N and n are the number of orbitals and the number of the occupied orbitals, respectively and E_i corresponds to the exact orbital. Figure 14 shows the condensation energy and the pairing energy level for the nanosize superconductivity. Note that the physical properties obtained in the mean-field approximation give a good description for the high DOS ($d \to \infty$). We have found the different behavior of the condensation energy from that obtained in the mean-field approximation, as shown in Fig. 14(a). Figure 14(b) presents the qualitative behavior of the pairing energy level in the ground state. At λ about 1.6, above two energy levels in Fig. 14(b) are completely paired. The pairing behavior has been already reported by many groups.[27,56]

Let us derive the exact equation for the Kondo regime in ultrasmall grains. We can consider the Hamiltonian $H = H_0 + H_1$ in Eq. (77). We introduce a creation operator describing all excited states at the spin singlet coupling between a conduction electron and a pseudofermion:

$$B_j^\dagger = \sum_{k,\sigma} \frac{c_{k\sigma}^\dagger f_\sigma}{\tilde{\varepsilon}_k - E_j}\,, \tag{92}$$

where E_j means the exact eigenenergies in the Kondo regime. The exact eigenstate $|\Psi_n\rangle$ for the Kondo regime can be written as $|\Psi_n\rangle = \Pi_{\nu=1}^n B_\nu^\dagger |0\rangle$. Other electrons, which are not related to the spin singlet order, contribute $E_{\rm single} = \sum_{k=1}^n \tilde{\varepsilon}_k$ to the eigenenergy. The ground state energy $E_{\rm GS}$ can be written as $E_{\rm GS} = \sum_{k=1}^n [E_k + \tilde{\varepsilon}_k]$.

By operating the Hamiltonian to the exact eigenstate, we obtain the condition:

$$1 + \sum_{k=1}^{N} \frac{\tilde{J}}{\tilde{\varepsilon}_k - E_j} = 0\,. \tag{93}$$

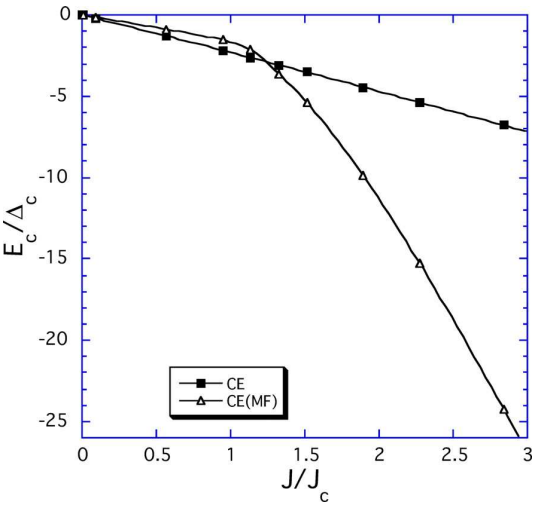

Fig. 15. Condensation energy for the Kondo regime: all parameters used in the system are as follows: eight energy levels, eight electrons, $d = 1.0$ and $\omega_D = 4.0$.

This equation gives the exact solution for the Kondo regime. Note that the creation operator (92) might be a true boson one as compared with the case of the reduced BCS model.

Figure 15 shows the condensation energy of the exact solution in the Kondo regime with that obtained in the mean-field approximation. We can find the different behavior of the condensation energy from that obtained in the mean-field approximation. However, the behavior is similar to that in the case of the superconductivity in nanosize systems.

We have investigated properties of the Kondo regime coupled to the superconductivity in ultrasmall grains by using the mean-field approximation. In the framework of the mean-field approximation, we have found the critical level spacing for the Kondo regime. The result suggests that the Kondo effect vanishes, when the level spacing becomes larger than the critical level spacing.

We have calculated physical properties of the critical level spacing and the condensation energy of the coupled system by using the mean-field approximation. From the results, we have found that strong local magnetic moments from the impurities make the transition temperature for superconductivity to be reduced. However, weak couplings λ of the superconductivity do not destroy the spin singlet order parameter at all. These results are in good agreement with the experimental results.[38] We have found that there is the coexistence region for both the superconductivity and the Kondo regime.

Finally, we have derived the exact equation for the Kondo regime in a nanosystem, which was not an easy task and have discussed the condensation energy from the viewpoint of energy levels. The further study of the properties in the Kondo regime with the use of the exact equation will be presented elsewhere.

In summary, we have investigated the Kondo effect and the superconductivity in ultrasmall grains by using a model which involves the *sd* and reduced BCS Hamiltonians with the introduction of a pseudofermion. The mean-field approximation for the model have been introduced, and we have calculated physical properties of the critical level spacing and the condensation energy. These physical properties have been discussed in relation to the coexistence of both the superconductivity and the Kondo regime. Finally, we have derived the exact equation for the Kondo regime in a nanosystem and discuss the condensation energy from the viewpoint of energy levels.

5. Interaction of Nanoscale Ferromagnetic Granules in Superconductor

Recent experiments have fabricated structured arrays of ferromagnetic nanoparticles in proximity to a bulk superconductor. We consider the theory of interactions between two nanoscale ferromagnetic particles embedded in a superconductor. In the London limit approximation, we will show that the interactions between ferromagnetic particles can lead to either parallel or antiparallel spin alignment. The crossover between these is dependent on the ratio of the interparticle spacing and the London penetration depth. We show that a phase transition between spin orientations can occur, as the temperature is varied. Finally, we comment on the extension of these results to arrays of nanoparticles in different geometries. We show that a phase transition between spin orientations can occur under variation of the temperature. Finally, we comment on the extension of these results to arrays of nanoparticles in different geometries.

Magnetism and superconductivity are two competing collective ordered states in metals. In the case of ferromagnetism, the exchange interactions lead to the parallel alignment of electronic spins, while electron–phonon interactions in the BCS superconductivity lead to the spin singlet pairing of electrons. Clearly, these two types of order are generally mutually incompatible. In bulk systems, the frustration between the electron singlet pairing and the spin ordering is resolved by the FFLO (Fulde–Ferrell,[57] Larkin–Ovchinnikov[58]) state. However, this has proved elusively experimentally, and few examples are known. In particular the FFLO state appears to be highly sensitive to disorder.

In recent years, however, there has been observed a great increase of the interest in the interactions between ferromagnetism and superconductivity in artificially structured systems. Advances in nanotechnology and microfabrication have made it possible to build hybrid structures containing both ferromagnetic and superconducting components which interact magnetically or via the proximity effect.[59,60] Superconductor–ferromagnetic–superconductor planar structures have been found to show the π-junction Josephson behavior.[61–63] Ferromagnet–superconductor–ferromagnet spin valve structures have also been fabricated[64] with potential applications to spintronics. More complex types of structures have also been produced;

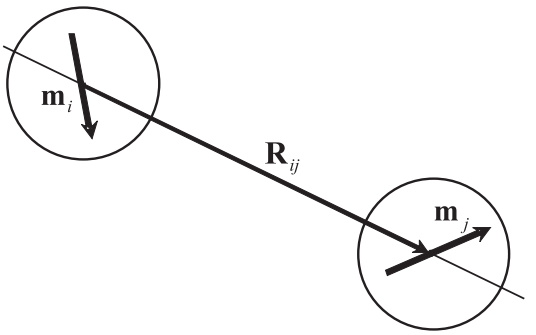

Fig. 16. Schematic diagram of a nanocomposite superconductor containing ferromagnetic granules.

for example, Moschalkov *et al.* fabricated arrays of ferromagnetic nanoscale dots on superconducting substrates.[65,66] A description of such structures based upon the Ginzburg–Landau theory was developed by Peeters.[67]

In this section, we consider the interaction between magnetic nanoparticles embedded in a superconductor, as shown in Fig. 16. Theoretical studies of such systems can be carried out exactly in two limiting cases depending on the relative magnitudes of the London penetration depth λ and the coherence length, ξ. If we consider the nanoparticles to be essentially point-like on the scale of both these characteristic lengths, then they correspond to effective point-like magnetic-moments of the form

$$\mathbf{M}(\mathbf{r}) = \sum_i \mathbf{m}_i \delta(\mathbf{r} - \mathbf{r}_i)\,, \tag{94}$$

where the particle at r_i has magnetic moment m_i. Interactions between these isolated moments arise directly from magnetic dipole–dipole forces modified by the screening of the bulk supercurrents. A second source of the interaction between the moments is the RKKY interaction modified by the presence of the BCS energy gap Δ. It is clear that the range of the dipolar forces is determined by the penetration depth λ, while the usual oscillatory power-law RKKY interaction is truncated exponentially on a length scale of the order of $\xi_{\mathfrak{w}}$. Therefore, the dipolar forces dominate for superconductors in the London limit $r_0 \ll \lambda$, while the RKKY interactions are more important in the Pippard case $r_0 \gg l$, where $r_0^{-1} = \xi_{\mathfrak{w}}^{-1} + l^{-1}$, and l (l–granular size, ξ–electron coherence length) is the mean free path.[68] Here, we consider the London limit and neglect RKKY interactions. Magnetic impurities interacting via RKKY interactions were considered by Larkin.[69] In the London limit, we first derive general expressions for the configuration of magnetic fields and the interaction energy of an ensemble of ferromagnetic granules. Then we consider the case of two interacting nanoparticles. It is found that, as a function of the temperature, an orientational phase transition can take place. The conditions for such a phase transition to occur are derived for a chain of ferromagnetic granules.

Finally, we comment on the application of these results to the determination of the equilibrium configurations of more general lattices of ferromagnetic particles.

5.1. *Magnetic field of ferromagnetic inclusions in a London superconductor*

We determine the magnetic configurations in superconducting nanocomposite systems by means of Maxwell's equations. The total current, $\mathbf{j}$, includes both normal and superconducting parts,

$$\mathbf{j} = \mathbf{j}_s + \mathbf{j}_n. \tag{95}$$

The role of the normal currents in a superconductor is negligible, since the superconductor exhibits weak magnetic characteristics in the normal state. However, a normal current will be present within the ferromagnetic inclusions. This normal-state current can be written in the traditional form

$$\mathbf{j}_n = \nabla \times \mathbf{M}\,, \tag{96}$$

where $\mathbf{M}$ is the magnetization of a material. The supercurrent obeys the usual London equation

$$\nabla \times \mathbf{j}_s = -\frac{n_s e^2}{m}\mathbf{B} \tag{97}$$

in SI units,[70] where $\mathbf{B}$ is the magnetic field, n_s is the superfluid density and m and e are the electron mass and charge, respectively.

Combining relations (95), (96), (97) with the Maxwell equation $\nabla \times \mathbf{B} = \mu_0 \mathbf{j}$, the magnetic field can be found in the form

$$\nabla \times (\nabla \times \mathbf{B}) + \lambda^{-2}\mathbf{B} = \mu_0 \nabla \times (\nabla \times \mathbf{M})\,, \tag{98}$$

where λ is the London penetration depth of the field in the superconductor. Since $\operatorname{div} \mathbf{B} = 0$, Eq. (98) can be rewritten as:

$$-\nabla^2 \mathbf{B} + \lambda^{-2}\mathbf{B} = \mu_0 \nabla \times (\nabla \times \mathbf{M})\,. \tag{99}$$

For the boundary conditions, we assume that the magnetic field in the superconductor vanishes far from the region of the ferromagnetic inclusions. According to these boundary conditions, the solution of Eq. (99) can be expressed as follows:

$$\mathbf{B}(\mathbf{r}) = \frac{\mu_0}{4\pi}\int d^3 r' G(|\mathbf{r} - \mathbf{r}'|) \nabla \times (\nabla \times \mathbf{M}(\mathbf{r}'))\,, \tag{100}$$

where the Green's function is given by:

$$G(|\mathbf{r} - \mathbf{r}'|) = \frac{\exp(-|\mathbf{r} - \mathbf{r}'|/\lambda)}{|\mathbf{r} - \mathbf{r}'|}\,. \tag{101}$$

After the double integration by parts and some algebraic manipulations, this expression can be rewritten in the general form:

$$\mathrm{B}(\mathbf{r}) = \frac{\mu_0}{4\pi}\int d^3r' \exp(-R/\lambda)\cdot\left\{\left(\frac{3\mathbf{R}(\mathbf{R}\cdot\mathbf{M}(\mathbf{r}'))}{R^5} - \frac{\mathbf{M}(\mathbf{r}')}{R^3}\right)\right.$$
$$\left.\times\left(1+\frac{R}{\lambda}+\frac{R^2}{\lambda^2}\right) - \frac{2\mathbf{R}(\mathbf{R}\cdot\mathbf{M}(\mathbf{r}'))}{\lambda^2\cdot R^3}\right\}, \tag{102}$$

where $\mathbf{r} = \mathbf{r} - \mathbf{r}', R = |\mathbf{r} - \mathbf{r}'|$.

Expression (102) determines the magnetic field outside of the ferromagnetic inclusions. Since the magnetization of the system $\mathbf{M}(\mathbf{r})$ is defined by (96), we have in (101) that $\mathbf{M}(\mathbf{r}) = 0$ outside of the volume of ferromagnetic granules.

5.2. *Magnetic field of ferromagnetic quantum dots in a superconducting nanocomposite material*

Assuming that the sizes of the ferromagnetic inclusions are on the nanometer length scale, they will appear essentially point-like on the scale of the penetration depth λ. In this case, we can approximate the magnetization as a sum of point magnetic moments, as shown in (94). Using this approximation in the general expression (102), we find the result (see Appendix B):

$$\mathrm{B}(\mathbf{r}) = \frac{\mu_0}{4\pi}\sum_i \exp(-R_i/\lambda)\cdot\left\{\left(\frac{3\mathbf{R}_i(\mathbf{R}_i\cdot\mathbf{m}_i)}{R_i^5} - \frac{\mathbf{m}_i}{R_i^3}\right)\right.$$
$$\left.\times\left(1+\frac{R_i}{\lambda}+\frac{R_i^2}{\lambda^2}\right) - \frac{2\mathbf{R}_i(\mathbf{R}_i\cdot\mathbf{m}_i)}{\lambda^2\cdot R_i^3}\right\}, \tag{103}$$

where $\mathbf{R}_i = \mathbf{r} - \mathbf{r}_i$ and $R_i = |\mathbf{r} - \mathbf{r}_i|$.

It is apparent from Eq. (103) that if the temperature of a superconductor approaches T_c, and the penetration depth $\lambda \to \infty$, then expression (103) tends to the limit

$$\mathbf{B}(\mathbf{r}) = \frac{\mu_0}{4\pi}\sum_i\left(\frac{3\mathbf{R}_i(\mathbf{R}_i\cdot\mathbf{m}_i)}{R_i^5} - \frac{\mathbf{m}_i}{R_i^3}\right), \tag{104}$$

which describes the usual magnetic field of isolated dipoles in the normal-state medium.

In the other limiting case, if the distance between granules is much more than the depth penetration, we have:

$$\mathbf{B}(\mathbf{r}) = \frac{\mu_0}{4\pi}\sum_i \frac{\exp(-R_i/\lambda)}{R_i\cdot\lambda^2}\cdot\left(\frac{\mathbf{R}_i(\mathbf{R}_i\cdot\mathbf{m}_i)}{R_i^2} - \mathbf{m}_i\right). \tag{105}$$

5.3. *Interaction energy of quantum dots in a superconducting nanocomposite material*

To determine the collective states of the magnetic moments in superconducting nanocomposite materials in the London limit, we make use the expression for the

free energy F of the system[71]

$$F = \frac{1}{2\mu_0} \int d^3r \{\mathrm{B}^2 + \lambda^2 (\nabla \times \mathbf{B})^2\} . \tag{106}$$

Integrating by parts and using the Gauss theorem, we transform Eq. (106) to the following form:

$$F = \frac{1}{2\mu_0} \int d^3r \, \mathbf{B}\{\mathbf{B} + \lambda^2 \nabla \times (\nabla \times \mathbf{B})\} = -2\pi\lambda^2 \int d^3r \, \mathbf{B} \cdot \nabla \times (\nabla \times \mathbf{M}) . \tag{107}$$

Integrating by parts and using the Gauss theorem again, we transform Eq. (107) to the form

$$F = -2\pi\lambda^2 \int d^3r \, \mathbf{M} \cdot \nabla \times (\nabla \times \mathbf{B}) . \tag{108}$$

Then, using the London Eq. (98) and omitting the magnetostatic self-energy from consideration, we find the interaction energy of magnetic moments. The obtained expression can be used to determine the collective state of magnetization of an ensemble of granules:

$$U = \frac{\mu_0}{8\pi} \sum_i \sum_j \exp(-R_{ij}/\lambda) \cdot \left\{ \left(\frac{3(\mathbf{R_{ij}} \cdot \mathbf{m_j})(\mathbf{R_{ij}} \cdot \mathbf{m}_i)}{R_{ij}^5} - \frac{\mathbf{m}_i \cdot \mathbf{m_j}}{R_{ij}^3} \right) \right.$$
$$\left. \times \left(1 + \frac{R_{ji}}{\lambda} + \frac{R_{ij}^2}{\lambda^2} \right) - \frac{2(\mathbf{R_{ij}} \cdot \mathbf{m_j})(\mathbf{R_{ij}} \cdot \mathbf{m}_i)}{\lambda^2 \cdot R_{ij}^3} \right\} , \tag{109}$$

where $\mathbf{r}_{ij} = \mathbf{r}_j - \mathbf{r}_i$, $R_{ij} = |\mathbf{r}_j - \mathbf{r}_i|$, $i \neq j$.

5.4. *Spin orientation phase transitions in a nanocomposite material with arrays of ferromagnetic quantum dots*

We begin by studying the magnetic configuration of an isolated pair of magnetic moments. The interaction energy of such a pair can be written as:

$$U = -\frac{\mu_0}{4\pi} \exp(-R_{12}/\lambda) \cdot \left\{ \left(\frac{3\,(\mathbf{R_{12}} \cdot \mathbf{m_1})\,(\mathbf{R_{12}} \cdot \mathbf{m_2})}{R_{12}^5} - \frac{\mathbf{m_2} \cdot \mathbf{m_1}}{R_{12}^3} \right) \right.$$
$$\left. \times \left(1 + \frac{R_{12}}{\lambda} + \frac{R_{12}^2}{\lambda^2} \right) - \frac{2(\mathbf{R_{12}} \cdot \mathbf{m_1})(\mathbf{R_{12}} \cdot \mathbf{m_2})}{\lambda^2 \cdot R_{12}^3} \right\} . \tag{110}$$

Let us introduce a coordinate system with the origin at the first magnetic moment $\mathbf{m}_1$ and the polar axis along the line connecting magnetic moments. In this coordinate system, the magnetic moments have the components $\mathbf{m}_i = m_i(\cos\varphi_i \sin\theta_i, \sin\varphi_i \sin\theta_i, \cos\theta_i)$ and their interaction energy (110) is written in the form:

$$U = \frac{\mu_0}{4\pi} m_1 m_2 \cdot \frac{\exp(-R_{12}/\lambda)}{R_{12}^3} \cdot f(\theta_i, \varphi_i, R_{12}/\lambda) , \tag{111}$$

where

$$f(\theta_i, \varphi_i, x) = -2(1+x)\cos\theta_1 \cos\theta_2 + (1+x+x^2)\sin\theta_1 \sin\theta_2 \cos\varphi \tag{112}$$

and $\varphi = \varphi_2 - \varphi_1$.

Differentiating the function $f(\theta_i, \varphi_i, x)$ with respect to angular variables and equating the results to zero, we find that there are four possible stable energy configurations:

$$\begin{gathered} \theta_1 = \theta_2 = 0\,, \\ \theta_1 = \theta_2 = \pi\,, \\ 0 \leqslant \varphi < 2\pi\,, \end{gathered} \tag{113}$$

$$\begin{gathered} \theta_1 = \theta_2 = \pi/2\,, \\ \varphi = \pi\,, \end{gathered} \tag{114}$$

$$\begin{gathered} \theta_1 = \theta_2 = \pi/2\,, \\ \varphi = 0\,, \end{gathered} \tag{115}$$

$$\begin{gathered} \theta_1 = 0, \quad \theta_2 = \pi\,, \\ 0 \leqslant \varphi < 2\pi\,, \end{gathered} \tag{116}$$

which are illustrated in Fig. 17.

The further analysis shows that configurations (115) and (116) are saddle points, not energy minima. Evaluating the second derivatives of (112), we obtain the stability condition of configuration (113):

$$\left(\frac{R}{\lambda}\right)^2 - \frac{R}{\lambda} - 1 \leqslant 0\,. \tag{117}$$

This implies that the ferromagnetic ordering of the pair of magnetic moments is possible if:

$$\frac{R}{\lambda} \leqslant \frac{1}{2}(1+\sqrt{5})\,. \tag{118}$$

It turns out that if condition (118) is violated, then the alternative configuration (114) is a stable energy minimum. We can conclude that if the temperature changes, and the penetration depth parameter $\lambda(T)$ varies in such a way that condition (118) is not satisfied, then the ground state orientation will change from (113) to (114).

This result is readily generalized to ordered arrays of ferromagnetic granules, and so we conclude that orientational phase transitions are possible in systems of quantum dots in a superconducting matrix. For example, it is clear that condition (118) can be applied to linear chains of quantum dots. On the other hand, the results for square or cubic lattices remain to be determined.

We have considered the interactions between nanoscale magnetic dots embedded in a bulk superconducting material. Our approach is valid for materials which are well described in the London limit $r_0 \ll \lambda$, since RKKY interactions are negligible. We have shown that, depending on the dimensionless parameter R/λ, different

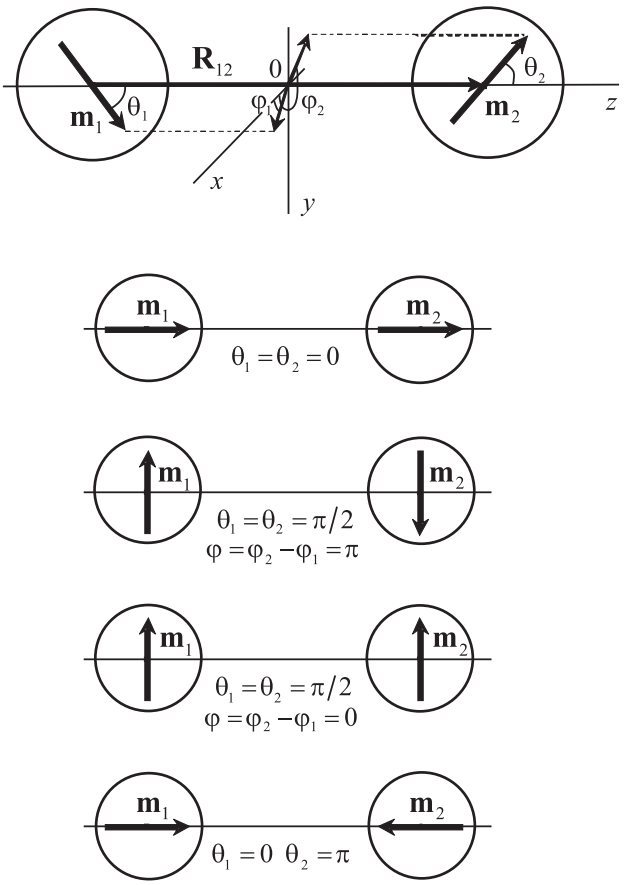

Fig. 17. Four energy saddle points of a pair of ferromagnetic quantum dots, as defined in (113). Of four, 1 and 2 correspond to the ground state, depending on condition (118). States 3 and 4 are never stable.

stable ground states occur. So, as the temperature varies, orientational phase transitions will take place for periodic arrays of such quantum dots. Of course, our calculation does not include all types of interactions which define the orientation of magnetic moments in space. In particular, we neglect the energy of a magnetic anisotropy of granules which is determined by the shape of granules or the type of their crystal lattice. However, when the shape of granules is close to the spherical one and the lattice of a ferromagnet has the cubic symmetry, then Eq. (109) will be essentially exact.

In the experimental systems studied by Moshchalkov,[66] a square of Pt/Co magnetic nanodots was deposited on the surface on the Pb superconductor, which is of type $I(k = 0.48)$. The dots were about 0.26 μm in diameter, and they were deposited on the grid with a spacing of 0.6 μm. For Pb, the penetration depth is 39 nm at low temperatures. So, this array was in the limit $R > \lambda$ and the dot–dot inter-

action would be expected to correspond to the antiferromagnetic alignment shown in the second state in Fig. 17. With increase in the temperature, the transition to the ferromagnetic alignment would occur according to Eq. (118) at $\lambda = 0.36\ R$, i.e., 219 nm.

According to the Casimir formula $\lambda(T) = \lambda(0)(1 - t^4)^{-1/2}$ with $t = T/T_c$, this would occur at $T = 7.14$ K, as compared with $T_c = 7.2$ K. Therefore, the experimental conditions for the transition to be observed are certainly feasible. Of course, for an exact comparison with theory in this case, our theory should be generalized to deal with magnetic particles near the surface rather than with those embedded in the bulk of a superconductor.

Of course, it would be interesting in the future to generalize our results to superconductors in the Pippard limit, where the RKKY interactions between quantum dots will dominate over dipolar forces.[69]

Expression (110) can be used to study, by means of numerical methods, the magnet configurations and the orientational phase transitions in an ensemble of nanogranules. It is possible to determine the conditions of orientational transformations in the analytic form for the ordered structures (a chain of granules, plane and volume lattices). Inasmuch as the state of the magnetic subsystem of a specimen at phase transitions is changed, this phenomenon can be experimentally observed under changing a magnetic susceptibility in the region of low fields.

6. Spin-orientation Phase Transition in Superconductors

In order to determine the collective state of magnetic moments in nanocomposite materials with the matrix made of a London-type superconductor, we use formula 103 for the energy of magnetic interaction.

First of all, we note that the realization of one or other magnetic configuration is defined by both the competition of diamagnetic effects from the side of the superconducting matrix and the magnetostatic interaction in the system of ferromagnetic granules. At lower temperatures eliminating the thermal disordering of the system, the magnetostatic interaction leads to a correlation of magnetic moments. As main conditions for the formation of magnetic configurations, we take the equivalence of all sites and the zero value of the net magnetic moment of the lattice. The planar lattice of granules by itself sets a preferred direction in space. Therefore, we will separate two configurations from the whole manifold of spatial orientations of magnetic moments. The first configuration is presented in Fig. 18. It is characterized by the orientation of the magnetization of granules which is orthogonal to the base plane. The alternation of the magnetization of neighboring granules decreases, to a certain extent, the energy of magnetic interaction. In addition, such a distribution of magnetic moments favors a decrease of the amplitude of a magnetic field in the superconducting matrix, which is also advantageous from the energy viewpoint. Thus, the given configuration can be considered as a version of the magnetic order.

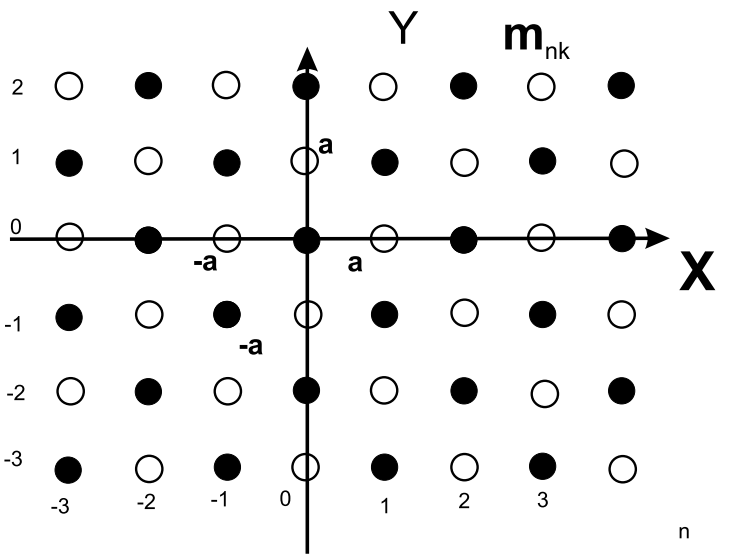

Fig. 18. Two-dimensional lattice of magnetic points. Magnetic moments (black color) are directed up or down (white color); a is the lattice constant.

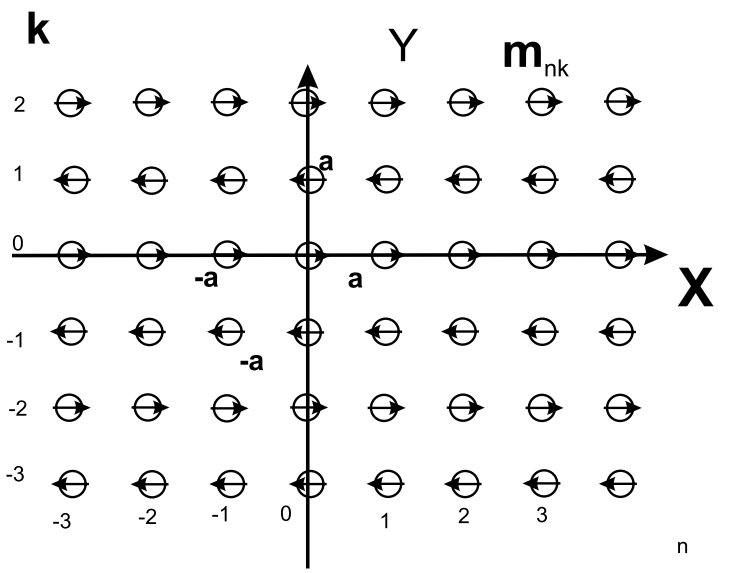

Fig. 19. Two-dimensional lattice of magnetic points. Magnetic moments are aligned in the plane in the form of chains; a is the lattice constant.

A configuration of the second type is shown in Fig. 19. It is characterized by the distribution of magnetic moments in the base plane of the lattice such that the magnetic moments are aligned as magnetic chains with alternating directions

of the magnetization. Here, like the configuration presented in Fig. 18, the main requirement, the equivalence of the states of magnetic points, is satisfied.

A similar distribution also decreases the energy of magnetostatic interaction, on the one hand, and favors a decrease in the amplitude of a magnetic field in a superconductor, on the other hand. At the same time, the planar orientation of magnetic moments has the basic distinction from the orthogonal one. For example, by means of a continuous deformation of the magnetization in the base plane, the configuration in Fig. 18 can be transferred into the structure shown in Fig. 19.

Such a system is characterized by a coherent rotation of magnetic moments by an angle $\pm\varphi$ relative to the principal direction of the lattice. In this case, there occurs both the modulation of the direction of moments at sites of the lattice and some increase in the energy of magnetic chains, but these processes are accompanied by the formation of magnetic vortices in cells, which promotes a decrease in the energy of magnetic interaction. The states of separate magnetic points in the lattice remain equivalent at the zero total magnetization.

Thus, the questions arise how the energy of the array of magnetic moments in the base plane shown in Fig. 20 depends on the angle $\pm\varphi$ and to which value it is equal in the equilibrium state. To answer these questions, we consider relation (110) for the interaction energy and reduce it to a single sum by virtue of the

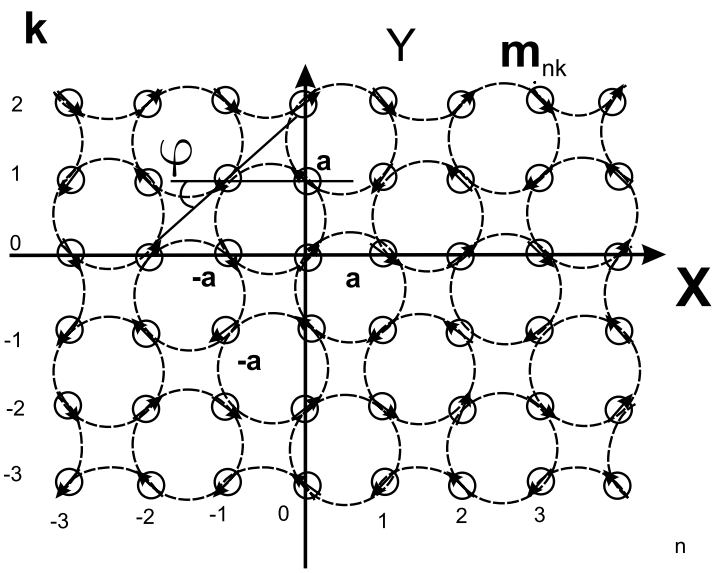

Fig. 20. Part of the lattice with a modulated planar distribution of the magnetization; a is the lattice constant. Circles stand for magnetic points, and the arrows on them indicate the directions of magnetic moments $m_n k$ in the base plane (n, k — the spatial indices of magnetic points). The angle φ defines the deviation of the moments of magnetic points from the principal direction of the lattice. The states of all points in the given configuration are equivalent. The net magnetic moment is zero. The separated circles denote schematically magnetic vortices. The dotted lines are tangents to the directions of magnetic moments at sites of the lattice.

fact that the states of magnetic points are equivalent. In this case, in order to calculate the energy of the lattice, it is sufficient to determine the energy of a single magnetic point, e.g., $m_{0,0}$, located at the origin of the coordinate system and then to multiply the result by the total number of magnetic points N. Relation (110) becomes significantly simpler:

$$U = -\frac{\mu_0}{4\pi}\frac{N}{2}\left\{3\left(1-\frac{\partial}{\partial\alpha}\right)+\frac{\partial^2}{\partial\alpha^2}\right\}\sum_i^N \exp(-\alpha\cdot r_i/\delta)\frac{(\mathbf{r}_i\cdot\mathbf{m}_i)(\mathbf{r}_i\cdot\mathbf{m}_{0,0})}{r_i^5}$$

$$+\frac{N}{2}\left\{1-\frac{\partial}{\partial\alpha}+\frac{\partial^2}{\partial\alpha^2}\right\}\sum_i^N \exp(-\alpha\cdot r_i/\delta)\frac{\mathbf{m}_i\cdot\mathbf{m}_{0,0}}{r_i^3}\,. \tag{119}$$

By writing formula (119), we used the method of differentiation with respect to the parameter α which should be set equal to 1 after the calculations. The index "i" stands for the summation over all sites of the lattice. Performing the summation in relation (119), it is convenient to introduce the pair of indices (n,k) defining the position of a site in the lattice (Fig. 20) instead of the running index of magnetic points "i". It is easy to see that the system represented in Fig. 20 *possesses* the translational invariance with a period of *2a* so that:

$$\begin{gathered}\mathbf{m}_{n,k}=\mathbf{m}_{n+2l,k+2p}\,,\\ l,p=\pm1,\pm2,\ldots\end{gathered} \tag{120}$$

The lattice has only four types of magnetic points differing from one another by a spatial orientation of magnetic moments. Their vector components depend on the angle φ in the following manner:

$$\mathbf{m}_{n,k}=\mathbf{m}_{n+2l,k+2p},\quad \mathbf{m}_{2l,2p}=\mathbf{m}_{0,0}=\begin{pmatrix}\cos\varphi\\ \sin\varphi\\ 0\end{pmatrix},$$

$$\mathbf{m}_{2l+1,2p}=\mathbf{m}_{1,0}=m\begin{pmatrix}\cos\varphi\\ -\sin\varphi\\ 0\end{pmatrix},$$

$$\mathbf{m}_{2l,2p+1}=\mathbf{m}_{0,1}=m\begin{pmatrix}-\cos\varphi\\ \sin\varphi\\ 0\end{pmatrix}, \tag{121}$$

$$\mathbf{m}_{2l+1,2p+1}=\mathbf{m}_{1,1}=m\begin{pmatrix}-\cos\varphi\\ -\sin\varphi\\ 0\end{pmatrix},$$

$$l,p=\pm1,\pm2,\ldots$$

$$l,p=\pm1,\pm2,\ldots\,,$$

where m is the modulus of the magnetic moment of a site.

After the substitution of (121) in (119) and the summation over sites of the unbounded lattice, we get the following interesting result. It turned out that the interaction energy of the system of magnetic points (see Fig. 20) does not depend on the angle φ and is determined by the relation

$$\frac{U_{\parallel}}{N} = \frac{\mu_0}{4\pi}\frac{m^2}{a^3} \cdot F(a/\delta)\,, \tag{122}$$

where N is the number of sites of the lattice, m is the magnetic moment of a granule, $F(a/\delta)$ is the energy characteristic of a magnetic state which is a universal function of a single parameter and determines the dependence of the energy on both the period and the field penetration depth in the case where the magnetic moments are distributed in the base plane of the lattice. It can be represented in the form of a sum

$$\begin{aligned} F(a/\delta) = \frac{\mu_0}{4\pi}\left(-1+\frac{\partial}{\partial\alpha}+\frac{\partial^2}{\partial\alpha^2}\right)\cdot\frac{1}{8}\sum_{l=1}^{\infty}\sum_{p=0}^{\infty}\frac{\exp(-2\alpha(a/\delta)\sqrt{l^2+p^2})}{(l^2+p^2)^{3/2}} \\ -\left(-1+\frac{\partial}{\partial\alpha}+\frac{\partial^2}{\partial\alpha^2}\right) \\ \cdot\frac{1}{4}\sum_{l=-\infty}^{\infty}\sum_{p=-\infty}^{\infty}\frac{\exp(-\alpha(a/\delta)\sqrt{(2l+1)^2+(2p+1)^2})}{((2l+1)^2+(2p+1)^2)^{3/2}} \\ -\left(3-3\frac{\partial}{\partial\alpha}+\frac{\partial^2}{\partial\alpha^2}\right) \\ \cdot\frac{1}{2}\sum_{l=-\infty}^{\infty}\sum_{p=-\infty}^{\infty}\frac{((2l+1)^2-(2p)^2)\cdot\exp(-\alpha(a/\delta)\sqrt{(2l+1)^2+(2p)^2})}{((2l+1)^2+(2p)^2)^{5/2}}\,. \end{aligned} \tag{123}$$

Thus, there occurs the degeneration of the state in the parameter φ in the presence of a tough correlation of the mutual orientations of moments of the ensemble of magnetic points. The energies of the configuration shown in Fig. 19(1b) and the ensemble with a modulated distribution of the magnetization (Fig. 20) coincide. In turn, the determination of the energy of magnetic interaction for the configuration possessing the orthogonal orientation of magnetic moments (Fig. 18) requires a smaller amount of calculations, because the first sum in formula (119) vanishes. The result of calculations can be represented in the form:

$$\frac{U_{\perp}}{N} = \frac{\mu_0}{4\pi}\frac{m^2}{a^3} \cdot \Phi(a/\delta)\,, \tag{124}$$

where $\Phi(a/\delta)$ is the energy characteristic of the magnetic state which a universal function of the single parameter and determines the dependence of the energy on both the period and the field penetration depth under the distribution of magnetic moments normally to the base plane of the lattice. This function can be represented

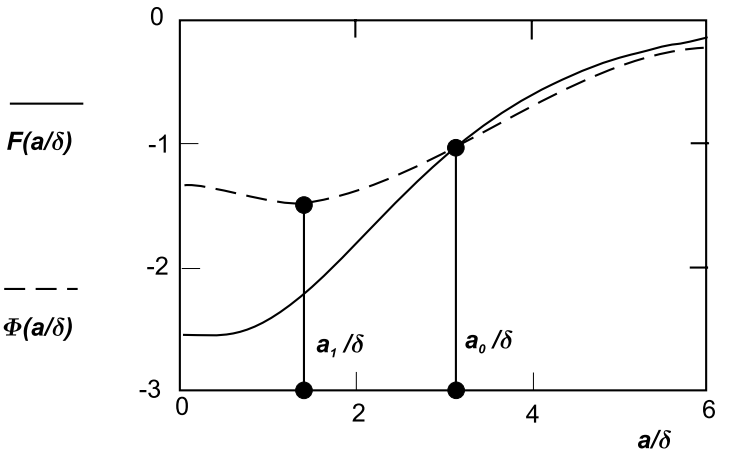

Fig. 21. Plots of the energy characteristics $F(a/\delta)$ and $\Phi(a/\delta)$ of states of the lattice with normal and planar orientations of magnetic moments, respectively. Values of $F(0)$ and $\Phi(0)$ correspond to the transition of the superconducting matrix into the normal state.

in the form:

$$\Phi(a/\delta) = \frac{\mu_0}{4\pi}\left(1 - \frac{\partial}{\partial\alpha} + \frac{\partial^2}{\partial\alpha^2}\right)\cdot\frac{1}{2}\cdot\left\{\sum_{l=1}^{\infty}\sum_{p=0}^{\infty}\frac{4\cdot\exp(-\alpha\cdot(a/\delta)\cdot\sqrt{2\cdot l^2+2\cdot p^2})}{(2\cdot l^2+2\cdot p^2)^{3/2}}\right.$$
$$\left. - \sum_{l=-\infty}^{\infty}\sum_{p=-\infty}^{\infty}\frac{\exp(-\alpha\cdot(a/\delta)\cdot\sqrt{2\cdot(l+1/2)^2+2\cdot(p+1/2)^2})}{(2\cdot(l+1/2)^2+2\cdot(p+1/2)^2)^{3/2}}\right\}. \tag{125}$$

The calculation of the functions (a/δ), $\Phi(a/\delta)$ on the basis of relations (123) and (125) is not a difficult task and can be realized with any mathematical software. The results are presented in the graphical form in Fig. 21.

In Fig. 21, we represent the plots of the energy characteristics of two different states of a magnetic lattice versus the ratio of the parameter of a cell and the penetration depth of the magnetic field, a/δ. The limit $a/\delta \to 0$ corresponds to the transition of the matrix into the normal state. It is obvious that a lattice with planar orientation of magnetic moments (Figs. 19 and 20) possesses the lower energy in the normal state at $a/\delta = 0$. Therefore, the state with the perpendicular direction of moments (Fig. 18) cannot be realized at all in the absence of a superconductor. As the temperature decreases and the penetration depth diminishes gradually, the parameter a/δ begins to grow. When this parameter attains the value $a_0/\delta \approx 3.3$, the configuration with the orthogonal orientation of magnetic moments (Fig. 18) becomes more advantageous in energy, and the orientation phase transition occurs in the system. At a decrease in the temperature, a similar scenario of events completely corresponds to a reorientation of the magnetic moments of an isolated pair of magnetic points which was considered in the previous work.[71]

In conclusion, we note that an analogous phase transition can be expected to occur in a planar lattice with rectangular cell. The only difference will consist in the elimination of the degeneration relative to the directions of magnetic moments in the base plane. Of course, the direct observation of a phase transition will be hampered, because the problem involves the magnetic lattice surrounded by a superconductor. However, a similar orientation transformation must happen also in a lattice applied on the surface of a massive superconductor, though values of the parameter a_0/δ will be different in this case.

7. Quantum Computer on Superconducting Qubits

7.1. *Principle of quantum computers*

Silicon microprocessors, being the main element of modern computers, have attained the limit of development. The miniaturization, i.e., the aspiration to place as much as possible components on a more and more smaller area of a chip, has approached the boundary of physical possibilities. Further, it will be impossible to conserve the stability of the operation of computers. Many researchers believe that silicon processors will begin to go into the past in at most five years, and the production of chips will be based on the other material — carbon nanotubes. It is worth noting that the computational processes are accompanied by the release of heat. R. Feynman said: "Any classical computation is a physical process running with the release of heat." As known, the calculations lead to an increase in the entropy and, hence, to the release of heat. The idea of the creation of quantum computers arose several decades ago, when it was proposed to reject the application of electric circuits in the processing of information and to pass to the use of quantum mechanics. The classical computers are processing the information only on the basis of ideas of one bit of information (it corresponds to the transition from state 0 to state 1 or conversely). The quantum computers can process the information, by basing on the ideas of a quantum bit (qubit) which allows one to realize simultaneously four logical operations ($0 + 0 = 0$, $0 + 1 = 1$, $1 + 0 = 1$, $1 + 1 = 2$).

Qubit is the abridged notation for quantum bit and means the unity of information coded in a quantum system which can be in the states $|0\rangle, |1\rangle$, and in any superposition of these states.

Let the state of a qubit be described by the state $|f\rangle$ which can be represented as a superposition of states $|0\rangle$ and $|1\rangle$:

$$|f\rangle = a|0\rangle + b|1\rangle\,,$$

where

$$a^2 + b^2 = 1\,. \tag{126}$$

Since the devices can register only classical quantities, the measurement of a quantum bit will give states $|0\rangle$ or $|1\rangle$ with probabilities determined by the squares of the coefficients a and b.

The use of the principle of superposition allows one to increase the informational space exponentially with linear growth of the size of a physical system, because the register including n qubits can be in a superposition of at once 2^n states.

In addition, quantum mechanics admits the existence of the so-called entangled states possessing no analogs in classical physics.

An ensemble of qubits is a collection of qubits in different but given states.

It is worth noting that, even on the level of mathematics, a quantum computer operates in a basically different way than that of a classical computer.

Input data are coded in "quantum cells of memory". In this case, the collection of qubits becomes a single quantum system. This system undergoes the sequence of elementary quantum operations. Quantum computations are a realization of the most astonishing idea to apply the principles of quantum mechanics to the world of computers. Ordinary computers, despite their complexity, use classical laws of mechanics. In the recent years, the theory of classical computations was developed on the basis of works by A. Turing. With the appearance of quantum computations, the new possibilities have arisen and the situation is radically changed. Quantum methods can be successfully used in the solution of mathematical problems, though the time consumed for the solution of mathematical problems increases exponentially with the complexity of a problem.

For the theory of quantum calculations, the physical nature of qubits is not of crucial importance; the basically important point is that the system in the course of calculations obeys the laws of quantum mechanics.

7.2. *Superconducting qubits*

The realization of a quantum computer requires the availability of systems with doubly degenerate ground state. For this reason, a great attention is paid to systems with two-level wells which can be fabricated by facilities of solid-state electronics. The modern technology allows one to produce circuits containing millions of transistors and Josephson junctions.

By observing the operation of electrical circuits at temperatures close to the absolute zero, the researchers found a new proof of the fact that the laws of quantum mechanics are suitable not only for the microscopic objects (atoms and electrons), but also for large electronic schemes which include superconducting bits (qubits).

Many years ago, the attempts to construct a Josephson computer on the basis of the Josephson tunnel logic hopelessly failed. The principal reason for the failure was the huge technological dispersion of parameters of tunnel junctions, which did not allow one to produce large microcircuits. A Josephson computer can be created only on the way having nothing in common with that based on semiconductors, namely it can be just a quantum computer.

The hope is related to two circumstances. First, the fabrication of superconducting qubits is quite possible in the framework of the up-to-date technology.

Second, the presence of a gap in the spectrum of excitations of a superconductor allows one to expect the suppression of generation in a system.

Let us consider the first steps on the way of the construction of a superconducting quantum computer. First, we consider, in brief, the Josephson effect.

7.3. *The Josephson effect*

The Josephson effect is certainly one of the most interesting phenomena in superconductivity. The Josephson effect consists in the passage of a superconducting current through a thin dielectric layer separating two superconductors (the so-called Josephson junction).

It was predicted by an English physicist B. Josephson on the basis of superconductivity theory (1962, Nobel's prize in 1973) and discovered experimentally in 1963. Conduction electrons pass through a dielectric (a film of copper oxide ~ 10 Å in thickness) due to the tunneling effect.[72,73]

In Fig. 22, we present a scheme of the Josephson tunneling between two superconductors. The Josephson stationary effect consists in that the superconducting current

$$J_c = J_0 \sin\varphi\,, \tag{127}$$

$$\frac{d\varphi}{dt} = \frac{2eV}{\hbar}\,, \tag{128}$$

where φ is the phase difference on the interface of superconductors, V is the applied voltage and J_0 is the critical current through the junction.

The Josephson effect indicates the existence of the electron ordering in superconductors, namely, the phase coherence: in the ground state, all electron pairs have the same phase φ characterizing their wavefunction $\Psi_1 = \sqrt{n_{s1}}e^{i\varphi_1}$. According to quantum mechanics, the presence of a phase difference must cause a current through the junction. The discovery of such a current in experiment proves the existence of macroscopic phenomena in the nature which are directly determined by the phase of a wavefunction.

$$\Psi = \sqrt{n}e^{i\psi}\,. \tag{129}$$

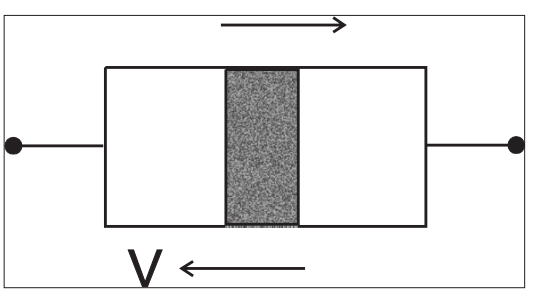

Fig. 22. Scheme of the Josephson tunneling between two superconductors.

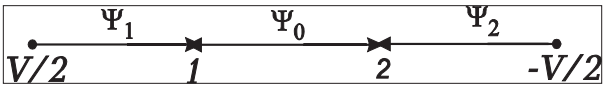

Fig. 23. Current passing through two series-connected Josephson junctions.

7.3.1. *Current passing through two series-connected Josephson junctions*

The Josephson current in the scheme drawn in Fig. 23 can be easily determined with the help of the elementary Feynman approach to a Josephson junction as a two-level quantum-mechanical system.[74] By introducing an intermediate object, some island, with the wavefunction Ψ_0 into the two-level system characterized by the wavefunctions $\Psi_1 = \sqrt{n_{s1}/2}e^{i\varphi_1}$ and $\Psi_2 = \sqrt{n_{s2}/2}e^{i\varphi_2}$, we write the Schrödinger equation in the form:

$$i\hbar\frac{d\Psi_1}{dt} = \frac{eV}{2}\Psi_1 + K\Psi_0\,, \tag{130}$$

$$i\hbar\frac{d\Psi_0}{dt} = K\Psi_1 + K\Psi_2 + E_0\Psi_0\,, \tag{131}$$

$$i\hbar\frac{d\Psi_2}{dt} = K\Psi_0 - \frac{eV}{2}\Psi_2\,. \tag{132}$$

The formula for a constant current running through two series-connected Josephson junctions at the zero external potential difference takes the form:

$$J = \hbar\frac{\partial\sqrt{n_{S1}}}{\partial t} = -\frac{K^2}{E_0}\sqrt{n_{S2}}\sin(\varphi_2 - \varphi_1)\,. \tag{133}$$

This relation can be rewritten as follows:

$$J_c = J_0\sin(\varphi)\,, \tag{134}$$

where $\varphi = \varphi_2 - \varphi_1$ is the phase difference. The relation obtained is named the Josephson formula (the Josephson stationary effect) and determines the current of superconductive electron pairs due to the tunneling transition.

The Josephson coupling energy is an important parameter of the Josephson junction. From (127), we have:

$$E = \int JV\,dt = \frac{hJ_0}{2}\int_0^{\pi}\sin\varphi d\varphi = -\frac{hJ_0}{2e}\cos\varphi\,. \tag{135}$$

The Josephson effect is still one of the phenomena that make superconductors such a fascinating area of study. Despite the more than 40-year intense studies and numerous applications, the Josephson effect remains an important field of researches in connection with the use of small superconducting grains.

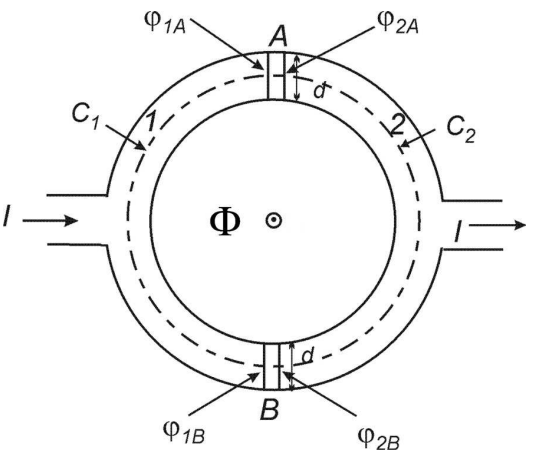

Fig. 24. Basic diagram of a "quantum interferometer".

7.3.2. *SQUIDS*

The Josephson effect allowed one to construct superconducting interferometers, SQUIDs (superconducting quantum interference device), which contain parallel weak connections between superconductors.[75] In Fig. 24, we present a scheme with Josephson junctions.

The total current running from 1 to 2 is equal to:

$$I = I_0 d[\sin(\Delta\varphi_1) + \sin(\Delta\varphi_2)]\,, \tag{136}$$

where

$$\Delta\varphi_1 = \varphi_{2A} - \varphi_{1A}\,,$$
$$\Delta\varphi_2 = \varphi_{2B} - \varphi_{1B}$$

are the phase differences on the first and the second Josephson junctions. There occurs a distinctive interference of the superconducting currents running through these connections.

Inside the superconductor, the current is zero $\mathbf{j} \equiv 0$. We will use the following formula for the current j:

$$\mathbf{j} \sim h\nabla\varphi - \frac{2e}{c}\mathbf{A}\,. \tag{137}$$

We can write:

$$\varphi_{1B} - \varphi_{1A} = \frac{2e}{hc}\int_{C_1} \mathbf{A}\cdot d\mathbf{l}\,, \tag{138}$$

$$\varphi_{2B} - \varphi_{2A} = \frac{2e}{hc}\int_{C_2} \mathbf{A}\cdot d\mathbf{l}\,. \tag{139}$$

Summing up these two equations, we get:

$$\varphi_{1B} - \varphi_{2B} + \varphi_{2A} - \varphi_{1A} = \frac{2e}{hc} \oint \mathbf{A} \cdot d\mathbf{l} = 2\pi \frac{\Phi}{\Phi_0} . \tag{140}$$

Thus, we have:

$$\Delta\varphi_1 - \Delta\varphi_2 = 2\pi \frac{\Phi}{\Phi_0} , \tag{141}$$

where Φ is the total quantum flux.

The flux quantum is defined as:

$$\Phi_0 = \frac{h}{2e} . \tag{142}$$

For a balance SQUID ring system, we can write:

$$\Delta\varphi_1 = \varphi_0 + \pi \frac{\Phi}{\Phi_0} ,$$

$$\Delta\varphi_2 = \varphi_0 - \pi \frac{\Phi}{\Phi_0} . \tag{143}$$

The total current in the SQUID is:

$$\begin{aligned} I &= I_0 \sin(\Delta\varphi_1) + I_0 \sin(\Delta\varphi_2) \\ &= I_0 \sin\left(\varphi_0 + \pi \frac{\Phi}{\Phi_0}\right) + I_0 \sin\left(\varphi_0 - \pi \frac{\Phi}{\Phi_0}\right) \\ &= 2I_0 \sin(\varphi_0) \cos\left(\pi \frac{\Phi}{\Phi_0}\right) = I_{\max} \left|\cos\left(\pi \frac{\Phi}{\Phi_0}\right)\right| \end{aligned} \tag{144}$$

with $I_{\max} = 2I_0 \sin(\varphi_0)$.

In this case, the critical current turns out to be periodically dependent on the flow of an external magnetic field, which allows one to use such a unit for the exact measurement of the magnetic field.

7.3.3. *Flux qubit*

Let us consider the first steps on the way of the creation of a superconducting computer. The simplest superconducting system demonstrating the coherency is SQUID which is a superconducting ring including a Josephson junction at one point. The energy of this system contains two terms — Josephson transition energy ($\cos\Phi$) and the energy related to the ring L:

$$H = -E_J \cos\left(2\pi \frac{\Phi}{\Phi_0}\right) + \frac{(\Phi - \Phi_x)^2}{2L} . \tag{145}$$

Here, Φ is the difference of superconductive phases at the junction. The superconductive phase in the ring is proportional to a magnetic flow applied to the ring

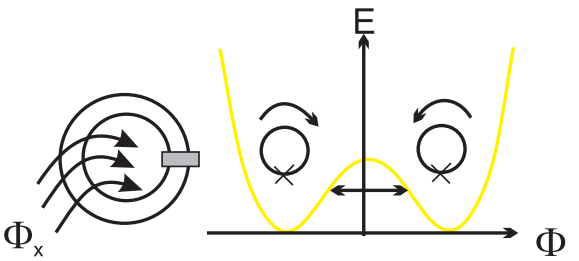

Fig. 25. Scheme of the Josephson tunneling between two superconductors.

(quantization of the magnetic flow). If Φ_x is equal exactly to a half of the magnetic flow, the potential of a SQUID becomes doubly degenerate:

Two minima of the well correspond to the currents in the ring passing in the clockwise ↻ and counterclockwise directions ↺, respectively.[76]

A superposition of these states in SQUID was observed experimentally in works.[76,77] These experiments demonstrated clearly the possibility to create a superposition of states in a system with a macroscopic number of particles. In the given case, the circular current including 10^{13} electrons was registered in a loop. The states participating in a superposition were macroscopically distinguishable, by differing from one another by the currents, whose difference was several microamperes. We indicate that, at the recent time, the important notion has been introduced in the course of studies of structures with Josephson junctions. It is the notion of macroscopic quantum coherence. In such systems, the Josephson energy can have two almost degenerate minima at values of the phase which are separated by a potential barrier (Fig. 25). It is possible that the phase passes from one minimum to another one due to the quantum-mechanical tunneling, and the eigenstates of the system are superpositions of the states localized in the first and second minima.

The operation of a superconducting computer requires low temperatures which are needed, in particular, to suppress heat-induced excitations destroying the quantum mechanical state of a system.

It is worth noting that the best condition for the observation of these current states is defined by a size of the superconducting ring. If the ring size is taken to be 1 cm, there appear the effects of decoherence which will destroy the current states. But if the ring is taken much smaller (say, 5 μm), then it is possible to observe these states. These states were discovered in experiments with Rabi oscillations.[77]

7.3.4. *Charge qubit*

The second type of a superconducting bit can be realized in the "Cooper pair box" system which is characterized by two charge states: without excess Cooper pair $|0\rangle$ and with a single Cooper pair $|1\rangle$. "Cooper pair box" is a nanotransistor with Coulomb blockage with controlling voltage V_g, as shown in Fig. 26. A "Cooper

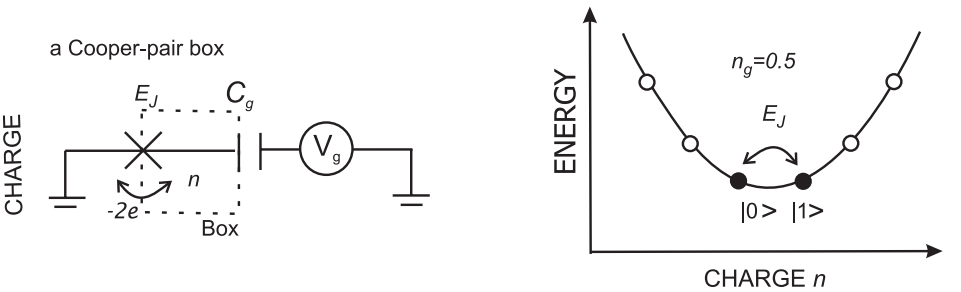

Fig. 26. Cooper-pair box [× denotes a Josephson junction (JJ)], C_g and V_g are the capacitor and the controlling voltage.

pair box" is represented by an aluminum superconducting film of the order of 1 mm in size with the working temperature of about several milli-Kelvin, which is significantly lower than the superconducting temperature T_c. Its quantum state can be characterized by the number of Cooper pairs. According to the BCS theory, the ground state of a superconductor is a superposition of states with different numbers of Cooper pairs. The excited, i.e., unpaired states in an ordinary superconductor are separated from the ground state by the energy gap. Therefore, as the number of electrons varies by 1, i.e., $N \to N \pm 1$, the ground state energy must be changed by $\pm\delta$. The sign (plus or minus) depends on that the initial number of electrons N is even or odd. The effects of parity of the number of electrons which are considered in this chapter in connection with mesoscopic superconductivity were successfully measured on nanotransistors with Coulomb blockage.

The Hamiltonian of such a system can be written as:

$$H = E_c(n - n_g)^2 + E_j \cos\varphi\,, \tag{146}$$

where E_c and E_j are the charging and Josephson energies and φ is the phase change. In the charging mode where $E_c \gg E_j$, only two lower charged states are of importance. The controlling voltage V_g induces a charge in the box

$$n_g = C_g \frac{V_g}{2e}\,, \tag{147}$$

where $2e$ is the charge of each Cooper pair and C_g is the gate capacitance. At $n_g = 1/2$, such a system operates as a two-level atomic system, in which the states $|0\rangle$ and $|1\rangle$ can be realized. The control is realized by a voltage V_g. On the basis of such a qubit, a system of two qubits was realized,[72,76] and the formation of entangled states was demonstrated. The effects of parity of the number of electrons which are considered in this chapter in connection with mesoscopic superconductivity were successfully measured on nanotransistors with Coulomb blockage.

7.3.5. *Phase qubit*

There exists one more possibility to realize SQUIDs with the use of high-temperature superconductors possessing the d-pairing (n-loop ones).[73]

The physics of d-pairing was considered in Ref. 73. Quantum processors on the base of these SQUIDs are developed at the Canadian company "D-wave".

We note also that, in addition to superconducting qubits, quantum computers use qubits possessing other physical properties. Scientists at the Yale University took a very fine aluminum plate in the fabrication of a quantum chip. A single qubit consists of one billion of aluminum atoms which behave themselves, nevertheless, as a single unit that can be in two energy states denoted as 0 and 1. Such quantum-mechanical states of a qubit cannot be long-term — their lifetime is about one microsecond. But it is sufficient for a chip to solve the so-called algorithm. We have considered the technologies of superconducting computers which represent a new type of quantum computers. These computers are based on the other mechanism obeying the laws of quantum mechanics. We recall that, till the recent time, the principle of devices was invariable and the archetype of such devices is mechanical clocks. In such devices, all stages of their relative motion can be observed; therefore, it is quite simple to understand their structure. On the contrary, the principle of operation of quantum computers involves the specific features of quantum mechanics which are difficult to understand. Nevertheless, by possessing the quantum resources, we can solve the very difficult complicated problems. In particular, the most important potential field of application of quantum computers is the problem of the exact calculation of properties of quantum systems.

Acknowledgment

We thank Professors V. Moshchalkov, K. Bennemann, N. Bogolyubov (Jr.), S. Aono and K. Yamaguchi for the fruitful discussions. S. K. is grateful for financial support to the SASIIU of the project Ukraine — Republic of Korea (2012).

References

1. J. Bardeen, L. N. Cooper and J. R. Schrieffer, *Phys. Rev.* **108**, 1175 (1957).
2. P. W. Anderson, *J. Phys. Chem. Solids* **11**, 26 (1959).
3. R. W. Richarson, *Phys. Lett.* **3**, 277 (1963).
4. K. A. Matveev and A. I. Larkin, *Phys. Rev. Lett.* **78**, 3749 (1997).
5. D. C. Ralph, C. T. Black and M. Tinkham, *Phys. Rev. Lett.* **78**, 4087 (1997).
6. M. Schechter *et al.*, *Phys. Rev. B* **63**, 214518 (2001).
7. G. Sierra, *Nucl. Phys. B* **572**, 517 (2000).
8. G. Stenuit *et al.*, *Eur. Phys. J B* **33**, 103 (2003).
9. A. Yu. Kasumov *et al.*. *Science* **284**, 1508 (1999).
10. K. H. Bennemann and J. B. Ketterson, *Superconductivity*, **1** (Springer, Heidelberg, 2008).
11. K. Clark *et al.*, *Nat. Nanotechnol.* **5**, 261 (2010).
12. H. Nagao, H. Kawabe and S. Kruchinin, Nanosize two-gap superconductivity, *Proc. NATO ARW Electron Correlation in New Materials and Nanosystems*, eds. K. Scharnberg and S. Kruchinin (Springer, Heidelberg, 2006), pp. 117–127.
13. H. Kawabe, H. Nagao and S. Kruchinin, Exact solution of two-band superconductivity, *Proc. NATO ARW Electron Correlation in New Materials and Nanosystems*, eds. K. Scharnberg and S. Kruchinin (Springer, Heidelberg, 2006), pp. 129–139.

14. H. Nagao and S. P. Kruchinin, Kondo effect coupled to superconductivity ultrasmall grains, *Proc. NATO ARW Electron Transport in Nanosystems*, eds. J. Bonca and S. Kruchinin (Springer, Heidelberg, 2008), pp. 105–115.
15. C. T. Black, D. C. Ralph and M. Tinkham, *Phys. Rev. Lett.* **76**, 688 (1996).
16. D. C. Ralph, C. T. Black and M. Tinkham, *Phys. Rev. Lett.* **74**, 3241 (1995).
17. B. Jankó, A. Smith and V. Ambegaokar, *Phys. Rev. B* **50**, 1152 (1994).
18. J. von Delft *et al.*, *Phys. Rev. Lett.* **77**, 3189 (1996).
19. R. A. Smith and V. Ambegaokar, *Phys. Rev. Lett.* **77**, 4962 (1996).
20. K. A. Matveev and A. L. Larkin, *Phys. Rev. Lett.*, **78**, 3749 (1997).
21. F. Braun and J. von Delft, *Phys. Rev. Lett.* **81**, 4712 (1998).
22. J. von Delft and F. Braun, *Phys. Rev. B* **59**, 9527 (1999).
23. V. N. Gladilin, V. M. Fomin and J. T. Devreese, *Solid State Comm.* **121**, 519 (2002).
24. G. Sierra *et al.*, *Phys. Rev. B* **61**, 11890 (2000).
25. R. W. Richardson and N. Sherman, *Nucl. Phys.* **523**, 253 (1964).
26. R. W. Richardson, *J. Math. Phys.* **6**, 1802 (1977).
27. R. W. Richardson, *Phys. Rev.* **141**, 949 (1966).
28. J. Nagamatsu *et al.*, *Nature* 410, 63 (2001).
29. L. Kouwenhoven and L. Glazman, *Phys. World* **14**(1), 33 (2001).
30. G. van der Wiel *et al.*, *Science* **289**, 2105 (2000).
31. T. Inoshita, *Science* **281**, 526 (1998).
32. S. Sasaki *et al.*, *Nature* (*London*) **405**, 764 (2000).
33. T. Inoshita *et al.*, *Phys. Rev. B* **48**, 114725(1993).
34. W. Izumida, O. Sakai and Y. Shimizu, *J. Phys. Soc. Jpn.* **67**, 2444 (1998).
35. A. L. Yeyati, F. Flores and A. Martin-Rodero, *Phys. Rev. Lett.* **83**, 600 (1999).
36. A. N. Pasupathy *et al.*, *Science* **306**, 86 (2004).
37. D. Matsubayashi and M. Eto, *Phys. Rev. B* **75**, 165319 (2007).
38. M. R. Buitelaar, T. Nussbaumer and C. Schönenberger, *Phys. Rev. Lett.* **89**, 256801 (2002).
39. A. Ueda and M. Eto, *Phys. Rev. B* **73**, 235353 (2006).
40. M. Eto and Y. V. Nazarov, *Phys. Rev. Lett.* **85**, 1306 (2000).
41. S. Reich *et al.*, *Phys. Rev. Lett.* **91**, 147001 (2003).
42. H. Suhl, B. T. Matthias and R. Walker, *Phys. Rev. Lett.* **3**, 552 (1959).
43. J. Kondo, *Prog. Theor. Phys.* **29**, 1 (1963).
44. K. Yamaji and Y. Shimoi, *Physica C* **222**, 349 (1994).
45. R. Combescot and X. Leyronas, *Phys. Rev. Lett.* **75**, 3732 (1995).
46. H. Nagao *et al.*, *Int. J. Quantum Chem.* **70**, 1075 (1988).
47. P. Konsin *et al.*, *Phys. Lett. A* **129**, 339 (1988).
48. P. Konsin and B. Sorkin, *Phys, Rev. B* **58**, 5795 (1998).
49. J. Kondo, *J. Phys. Soc. Jpn.* **70**, 808 (2001).
50. J. Kondo. *J. Phys. Soc. Jpn.* **71**, 1353 (2002).
51. S. P. Kruchinin and H. Nagao, *Phys. Part. Nuclei* **36**, 127 (2005).
52. D. L. Cox and M. B. Maple, *Phys. Today* **48**(2), 32 (1995).
53. A. C. Hewson, *The Kondo Problem to Heavy Fermion* (Cambridge, England, 1993).
54. A. Yoshimori and A. Sakurai, *Suppl. Prog. Theor. Phys.* **46**, 162 (1970).
55. M. Eto and Y. V. Nazarov, *Phys. Rev. B* **64**, 85322 (2001).
56. H. Nagao *et al.*, *Int. J. Quantum Chem.* **75**, 549 (1999).
57. P. Fulde and A. Ferrell, *Phys. Rev.* **135**, A550 (1964).
58. A. Larkin and Y. Ovchinnikov, *Sov. Phys. JETP* **20**, 762 (1965).
59. I. F. Lyuksyutov and V. L. Pokrovsky, *Adv. Phys.* **54**, 67 (2005).
60. A. F. Andreev, *Usp. Phys.* **168**(6) 656 (1998).

61. V. V. Ryazanov *et al.*, *Phys. Rev. Lett.* **86**, 2427 (2001).
62. S. M. Frolov *et al.*, *Phys. Rev. B* **70**, 144505 (2004).
63. C. Bell *et al.*, *Phys. Rev. B* **71**, 180501 (2005).
64. A. Ruotolo *et al.*, *Supercond. Sci. Technol.* **18**, 921 (2005).
65. M. Lange *et al.*, New Trends in Superconductivity, *NATO Sci. Series II Math. Phys. Chem.* Vol. 67, eds. J. F. Annett and S. Kruchinin (Kluwer, Dordrecht, 2002), p. 365.
66. A. Yu. *et al.*, *Supercond. Sci. Technol.* **22**, 1 (2009).
67. M. V. Milosovec and F. M. Peeters, *Europhys. Lett.* **70**, 670 (2005).
68. L. A. Fetter and J. D. Walecka, *Quantum Theory of Many-Particle Systems* (McGraw-Hill, Singapore, 1987).
69. V. M. Fetter and A. I. Larkin, *Phys. Rev. B* **66**, 64526 (2002).
70. J. F. Annet, *Superconductivity, Superfluids and Condensates*, (University of Bristol, Oxford University Press, 2003), p. 183.
71. M. V. Milosevic, S. V. Yampolskii and F. M. Peeters, *Phys. Rev. B* **66**, 174519 (2002).
72. Y. Nakamura, Y. A. Pashkin and J. S. Tsai, *Nature*, **398**, 786 (1999).
73. Y. Makhlin, G. Schon and A. Shnirman, *Rev. Mod. Phys.* **73**, 357 (2001).
74. R. P. Feynman, *Statistical Mechanics*, (Addison Wesley, Redwood City, 1982).
75. P.-G. de Gennes, *Superconductivity of Metals and Alloys* (Addision. Wesley, Advanced Book Programme, 1966).
76. J. Q. You and F. Nori, *Phys. Today*, **12**, 42 (2005).
77. I. Chiorescu *et al.*, *Science* **299**, 1869 (2003).